



OPEN Synergistic impact of mesoporous Zn/Al-LDH nanorods for developing dielectric and thermal properties of epoxy as insulation in GIS/GIL

M. Ramadan¹✉, Mahmoud Ezzat², Mousa. A. Abd-Allah², S. M. A. El-Gamal¹ & Abdelrahman Said^{2,3}✉

Gas-insulated switchgear (GIS) and transmission lines (GIL) depend on epoxy spacers to ensure electrical reliability under high-voltage stress. Yet, the limited dielectric strength and thermal tolerance of neat epoxy constrain its long-term applicability. This work investigates Zn/Al layered double hydroxide (LDH) nanoparticles as functional fillers for epoxy insulation. The nanofillers were synthesized by co-precipitation, surface-functionalized for improved compatibility, and incorporated into epoxy at loadings of 1–7 wt%. Structural, thermal, dielectric, and breakdown properties were systematically assessed. The Zn/Al-LDH exhibited a mesoporous nanostructure with high surface area (~98.9 m²/g) and uniform dispersion in the matrix, increasing epoxy structural ordering from 21.1% to 28.9%. Thermal stability improved as the char yield rose from 14% (neat epoxy) to 17.1% at 5 wt%, while the glass transition temperature shifted from 93.5 °C to 109.8 °C, surpassing the IEC 62271-1 limit. Dielectric analysis confirmed stable permittivity, low loss at 50 Hz, and suppressed DC conductivity down to 10⁻¹⁵–10⁻¹² S/cm. Most notably, breakdown strength rose from 30.08 kV/mm in neat epoxy to 37.42 kV/mm at 5 wt%, representing a 24% enhancement and the most reliable statistical profile under Weibull analysis. Beyond this concentration, agglomeration effects reversed the benefits, lowering performance below that of pure epoxy. These findings highlight Zn/Al-LDH/epoxy nanocomposites as a promising class of advanced insulating materials, with optimum performance achieved at 3–5 wt% loading. The combined improvements in dielectric reliability, thermal stability, and breakdown endurance demonstrate their potential for next-generation GIS/GIL applications.

Keywords Layered double hydroxide, Nanoparticles, Epoxy resin, Dielectric reliability, Breakdown strength

Gas-Insulated Switchgear (GIS) and Gas-Insulated Transmission Lines (GIL) are essential components of modern high-voltage power networks. Their importance arises from their compact design, high operational reliability, and safe performance in space-constrained environments. The increasing use of GIS/GIL in urban substations and critical grid nodes reflects the need for materials that provide high dielectric strength while keeping the equipment footprint small¹. In these systems, sulfur hexafluoride (SF₆) or SF₆-based gas mixtures serve as the primary insulating medium. In contrast, epoxy spacers play a dual role: they hold the conductors in position and manage the local gas–solid dielectric interface, which strongly influences field distribution and insulation reliability under electrical stress².

Epoxy has long been the material of choice for spacers in GIS/GIL because it combines electrical insulation strength, mechanical robustness, chemical stability, and the ability to be moulded into complex geometries. Moreover, epoxy bonds well with metallic inserts, which are essential for maintaining the electro-mechanical stability of spacer assemblies. To further improve its performance, researchers have investigated epoxy nanocomposites. The addition of carefully selected inorganic nanofillers can adjust interfacial polarization and trap energy levels, suppress conductivity growth, and enhance resistance to electrical ageing provided that filler type, loading, and dispersion are well controlled^{2–4}.

¹Chemistry Department, Faculty of Science, Ain Shams University, Cairo 11566, Egypt. ²Department of Electrical Engineering, Faculty of Engineering at Shoubra, Benha University, Cairo 11672, Egypt. ³Faculty of Computer Science, Benha National University (BNU), Al Obour, Egypt. ✉email: M.Ramadan@Sci.asu.edu.eg; abdelrahman.ghoniem@feng.bu.edu.eg; abdelrahman.ghoniem@cs.bnu.edu.eg

Initial efforts using micro-scale fillers such as SiO₂ and Al₂O₃ primarily targeted improvements in mechanical strength and mitigation of thermal expansion mismatch in epoxy composites. However, these systems delivered only limited gains in electrical performance. The emergence of nanotechnology has since enabled transformative advances. Nanofillers including SiO₂, Al₂O₃, TiO₂, and ZrO₂ exhibit strong interfacial interactions even at low concentrations, which can significantly influence dielectric permittivity (ϵ'), loss tangent ($\tan \delta$), trap distribution, and breakdown strength².

The electrical performance of nanofilled epoxy systems is highly sensitive to filler composition and loading. For instance, epoxy/SiO₂ composites at 3–5 wt% exhibited a decline in DC breakdown strength, while epoxy/MgO systems at similar concentrations showed marked improvement. Epoxy/Al₂O₃ nanocomposites also demonstrated enhanced breakdown behavior, attributed to the formation of well-dispersed particle networks that suppress charge accumulation and disrupt discharge pathways³. These findings highlight the importance of optimizing both filler morphology and concentration, as excessive loading or poor dispersion can lead to agglomeration and void formation ultimately compromising electrical reliability.

The dielectric properties of epoxy strongly govern its suitability as an insulating matrix, and numerous reports have explored how nanofillers alter the relative permittivity (ϵ'), dielectric loss ($\tan \delta$), and electrical conductivity (σ). Neat epoxy typically exhibits a very low conductivity in the order of 10⁻¹⁶ to 10⁻¹⁵ S m⁻¹ and a high relative permittivity at low frequencies such as 50 Hz⁴. When high-permittivity ceramics are introduced, substantial improvements are observed. For example, epoxy/BaTiO₃ composites at 0.5 volume fraction displayed ϵ' values exceeding 40, compared with values below 10 for the neat resin. However, this increase is coupled with higher losses; $\tan \delta$ values may rise above 0.1 at high filler contents⁵.

In contrast, oxide nanofillers such as SiO₂ often suppress ϵ' , $\tan \delta$, and σ at modest loadings^{2,3,6}. For instance, epoxy with 5 wt% SiO₂ exhibited lower permittivity and loss than the neat system, whereas increasing to 10 wt% reversed this trend and led to higher values⁷. These contrasting behaviors underscore the importance of filler selection and optimization in tailoring epoxy-based insulation systems for specific electrical performance requirements.

Frequency-dependent studies further reveal characteristic relaxation signatures, with $\tan \delta$ minima near 10² Hz and growth toward the MHz range. Similar interfacial immobilization effects are reported for Al₂O₃/epoxy, where ϵ' decreases at ~1 wt% due to rigid interfacial layers, rises at 2–4 wt%, and then falls again beyond 5 wt%⁸. These trends underscore the dual role of nanofillers: high-permittivity ceramics can significantly elevate ϵ' , while oxide-based fillers tend to suppress dielectric loss and conductivity by restricting interfacial polarization. Nevertheless, the overall dielectric response remains highly sensitive to filler type, loading concentration, and interfacial compatibility, necessitating careful optimization for targeted insulation performance.

Among oxide nanofillers, systems based on SiO₂, TiO₂, and Al₂O₃ have shown improved breakdown strength and reduced dielectric loss when particle size and surface chemistry are optimized. Surface functionalization (for example, with silane coupling agents like APTES) further enhances performance by improving filler dispersion and introducing chemical groups that act as carrier traps. Particle size is also critical; studies on TiO₂-based nanocomposites showed that smaller nanoparticles provided higher breakdown strength compared with larger particles, highlighting the influence of interfacial area and defect statistics⁶.

Thermal characterization of epoxy nanocomposites reveals that neat epoxy typically undergoes initial degradation between 300–350 °C, with major weight loss occurring from 350–450 °C. The incorporation of nanofillers can effectively delay thermal degradation onset and increase char yield, although inadequate dispersion may negate these benefits. Differential scanning calorimetry (DSC) places the glass transition temperature (T_g) of neat epoxy within the range of 72–99 °C. Numerous studies have shown that nanofillers such as SiO₂, Al₂O₃, TiO₂, and LDH not only elevate T_g but also reduce the heat capacity change (ΔC_p), indicating restricted polymer chain mobility. Overall, thermal enhancements are evident but remain highly dependent on filler type, concentration, and dispersion quality⁶.

Layered double hydroxide (LDH) nanofillers have garnered significant attention due to their unique lamellar morphology and tunable chemical composition. These features enable precise modulation of trap states within epoxy matrices, positioning LDH as a promising additive for suppressing surface charge accumulation and enhancing dielectric reliability in GIS spacer applications⁹.

Recent studies have established LDH nanofillers as multifunctional additives capable of improving both the dielectric and thermal behavior of epoxy systems. Huan et al.¹⁰ have demonstrated that silane-modified LDH particles suppress electrode charge injection and reduce field distortion by optimizing trap energy distributions, thereby enhancing insulation reliability. Similarly, Liu et al.¹¹ have integrated Mg/Al-LDH-coated silica spheres into epoxy coatings, achieving superior thermal insulation and flame retardancy, confirming the multifunctional potential of LDH structures. Moreover, integrated experimental and simulation evidence has demonstrated that Zn/Al-LDH nanofillers effectively suppress surface charge accumulation and enhance flashover voltage in GIS spacers, linking material-level improvements with system-level insulation reliability¹². Despite these advancements, studies exploring the mesoporous Zn/Al-LDH nanorods architecture in epoxy matrices remain scarce, particularly concerning its combined influence on dielectric reliability, thermal stability, and breakdown strength which forms the central focus of the present work.

Therefore, this study aims to develop high-performance epoxy-based insulating materials for GIS and GIL applications by incorporating mesoporous Zn/Al layered double hydroxide (LDH) nanorods. The work focuses on enhancing overall insulation reliability, combining superior dielectric and thermal performance with improved breakdown strength, thereby addressing the inherent limitations of neat epoxy under high-voltage stress and advancing the design of next-generation insulation systems.

Material	IUPAC name	Purity (%)	Producer (City, Country)
Epoxy resin	Bisphenol-A diglycidyl ether (DGEBA)	–	Chemicals for Modern Building International, Giza, Egypt
Hardener	Polyamine curing agent	–	Chemicals for Modern Building International, Giza, Egypt
Zinc nitrate	Zinc nitrate hexahydrate	98%	Sigma-Aldrich, St. Louis, USA
Aluminum chloride	Aluminum chloride	99.999%	Sigma-Aldrich, St. Louis, USA
Sodium carbonate	Sodium carbonate	≥ 99.5%	Sigma-Aldrich, St. Louis, USA
Silane coupling agent	(3-Aminopropyl) triethoxysilane (APTES)	99%	Sigma-Aldrich, St. Louis, USA
Ethanol	Ethanol	99%	El Nasr Pharmaceutical Chemicals, Cairo, Egypt

Table 1. Chemicals specifications used in this study.

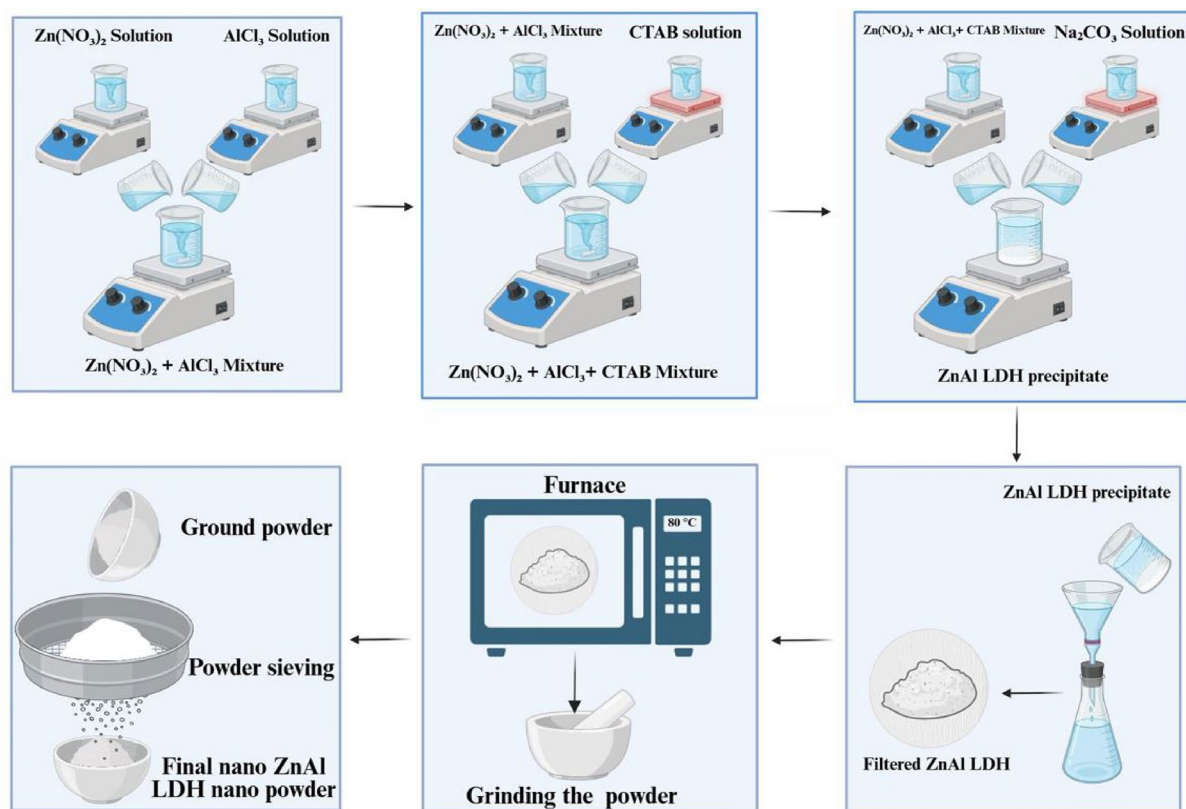


Fig. 1. A full description of the nano material preparation process.

Materials

The base epoxy used in this work is KEMAPOXY 150 JM (Chemicals for Modern Building International, Giza, Egypt), a two-component, solvent-free liquid epoxy formulated for electrical insulation. It complies with ASTM D150, ASTM D257, and ASTM D495 standards, with a density of 1.15 ± 0.02 kg/L at 25 °C. It consists of two Components, the epoxy A and the hardener B, which were mixed in a 3:1 weight ratio, providing a pot life of ~45 min, initial setting within 10–12 h, and complete curing after 7 days. The specifications of all the chemicals used in this study are listed in Table 1.

Preparation of Zn/Al-LDH nanofillers

Zn–Al layered double hydroxide (Zn–Al–CO₃ LDH) was synthesized by the co-precipitation method. Equimolar solutions of zinc nitrate [$\text{Zn}(\text{NO}_3)_2$, 0.5 M] and anhydrous aluminium chloride [AlCl_3 , 0.5 M] were prepared in a 2:1 molar ratio and stirred magnetically for 15 min to ensure homogeneity. A 2 M sodium carbonate solution was then added dropwise to the mixture until a white precipitate formed at pH 7–8. The obtained precipitate was filtered, thoroughly washed with distilled water, and dried overnight at 80 °C. Finally, the dried product was ground and sieved to obtain Zn–Al–CO₃ LDH powder. A full description of the Zn/Al-LDH preparation process is illustrated in Fig. 1.

Surface functionalization of nanoparticles

Surface functionalization of nanoparticles is an effective strategy to enhance their dispersibility in epoxy matrices by reducing surface energy and improving compatibility with the polymer. Unlike physical treatments, which are unstable under heat or solvents, chemical modification using coupling agents such as silane (APTES) provides stable and durable interfaces, as shown in Fig. 2. These agents form bonds both with the nanoparticle surface and the polymer chains, reducing hydrophilicity and promoting uniform dispersion. As a result, functionalization improves interfacial adhesion and tailors the bulk properties of nanocomposites⁶.

The functionalization process of the nanoparticles was initiated by dispersing 3 g of the prepared powder in 60 mL of ethanol within a round-bottom flask. The suspension underwent ultrasonication at 70 °C for 30 min to disintegrate agglomerates and achieve uniform dispersion, followed by mechanical stirring at 500 rpm for 30 min under the same conditions. A 10% (w/w) solution of 3-aminopropyltriethoxysilane APTES in ethanol was subsequently added dropwise while stirring continued, and the reaction mixture was maintained for 5 h to promote effective grafting of silane molecules onto the nanoparticle surfaces. After completion, the product was recovered by filtration, washed thoroughly with ethanol to eliminate unreacted silane, and dried at 80 °C overnight, resulting in silane-modified nanoparticles suitable for incorporation into the epoxy matrix¹³.

Preparation of epoxy Zn/Al-LDH nanocomposite

The epoxy-based nanocomposites were prepared through a multi-step procedure. Initially, the synthesized Zn/Al-LDH nanoparticles were dried at 80 °C overnight to remove residual moisture, then dispersed in ethanol and ultrasonicated for 60 min to achieve uniform suspension. The obtained dispersion was gradually introduced into epoxy resin under continuous stirring for 2 h, followed by an additional ultrasonication step (30 min) and mechanical stirring (2 h) to improve homogeneity. Residual ethanol was eliminated by heating the mixture at 80 °C until constant weight was achieved. The solvent-free epoxy/nanoparticle mixture was then blended with the hardener at a 3:1 weight ratio, stirred for 3 min, and degassed on a hot plate to remove entrapped air bubbles. Finally, the mixture was cast into pre-prepared molds and cured under ambient conditions for 24 h to obtain the nanocomposite samples. A schematic illustration of the key preparation stages is presented in Fig. 3.

Methodology

After the preparation of Zn/Al-LDH nanoparticles and epoxy resin nanocomposites at different loadings (1, 3, 5, and 7%wt.), a series of characterization and performance evaluations were carried out for both nanomaterials and nanocomposites.

Nanoparticle characterization

The morphology of Zn/Al-LDH nanoparticles was examined using a High Resolution Transmission Electron Microscope coupled with Selected Area Electron Diffraction (HRTEM/SAED, Model 2100 Plus, JEOL Ltd., Tokyo, Japan) operated at 200 kV to determine particle size, dispersion state and crystallographic structure. The degree of crystallinity and phase composition were confirmed by X-ray Diffraction (XRD, Model X'Pert PRO, PANalytical B.V., Almelo, Netherlands) using Cu K α radiation ($\lambda = 1.5406 \text{ \AA}$), scanned in the 2θ range of 5–70° with a step size of 0.02° equipped with Cu K α radiation ($\lambda = 1.5406 \text{ \AA}$), operated at 40 kV and 30 mA. The scans were recorded in Bragg–Brentano geometry over a 2θ range of 5–70° with a step size of 0.02° and scan rate of 2°/min. In addition, all textural parameters of synthesized nanoparticles were evaluated via nitrogen adsorption desorption technique. Surface area and porosity measurements were performed using a Micromeritics ASAP 2020 Plus Accelerated Surface Area and Porosimetry System (Micromeritics Instrument Corp., Norcross, GA, USA).

Nanocomposite characterization

The microstructure of the epoxy Zn/Al-LDH nanocomposites was observed by Scanning Electron Microscopy equipped with Energy Dispersive X-ray Spectroscopy using (SEM, Model Quanta 250, FEI Company, Hillsboro, USA, equipped with EDX, Oxford Instruments, Abingdon, UK) to assess nanoparticle dispersion and elemental

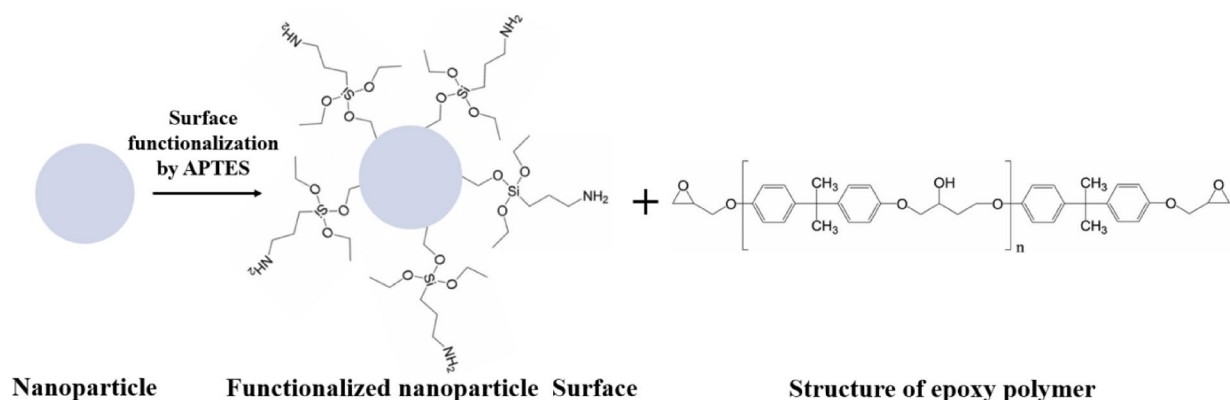


Fig. 2. Surface functionalization process.

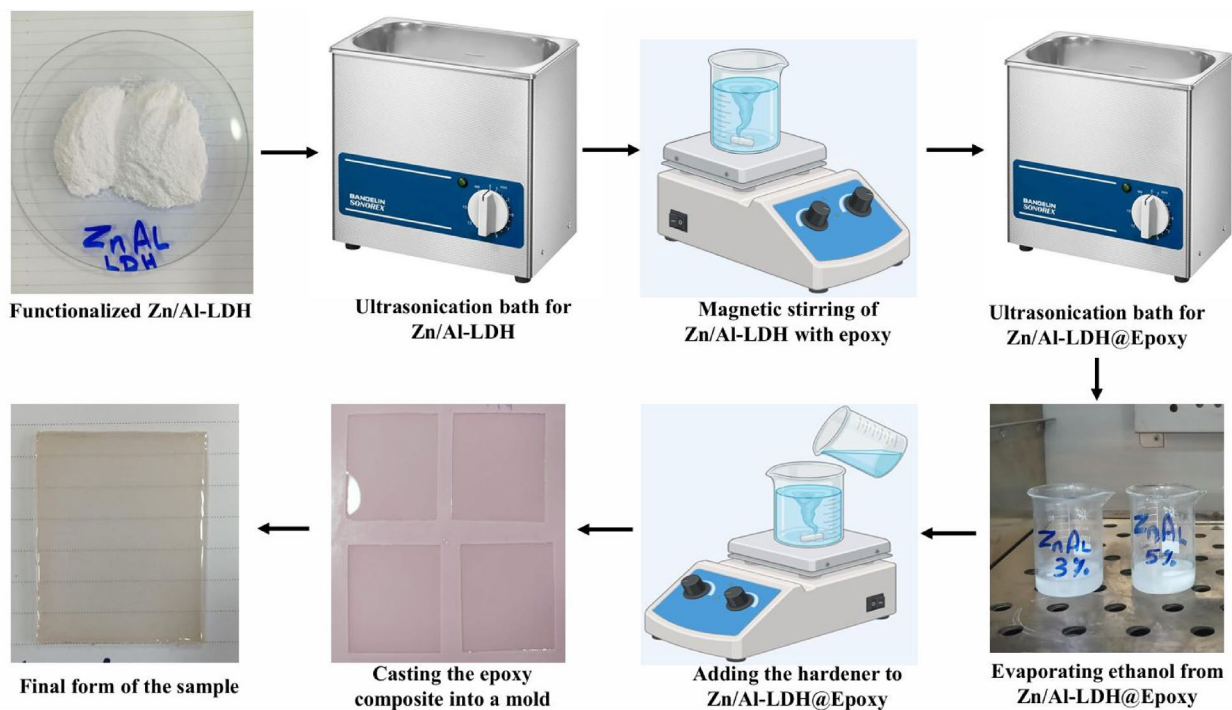


Fig. 3. A schematic illustration of the key preparation stages.

composition. Complementary XRD measurements were also carried out on the composites to investigate any structural modifications upon filler incorporation.

Thermal analysis

The thermal behavior of the optimized nanocomposite formulation (corresponding to the loading that exhibited the highest breakdown strength) was evaluated using Thermogravimetric Analysis (TGA/DSC Analyzer, THEMYSYS ONE, Setaram Instrumentation, Caluire-et-Cuire, France). Tests were conducted from room temperature up to 700 °C at a heating rate of 15 °C/min under nitrogen flow. TGA was used to study thermal stability and degradation profiles, while DSC provided the glass transition temperature (T_g) of the composites. The second heating run was used to eliminate any residual solvent or absorbed moisture effects. The recorded heat flow values were normalized to the polymer mass fraction.

Dielectric properties

Dielectric measurements, including relative permittivity (ϵ_r), dielectric loss tangent ($\tan \delta$), and AC conductivity, were performed using (Dielectric Spectrometer, Alpha-A Analyzer with Concept 40 Interface, Novocontrol Technologies GmbH & Co. KG, Montabaur, Germany). Impedance and dielectric spectroscopy were performed using a parallel-plate electrode system integrated inside the Novocontrol sample cell, which is the standard configuration recommended for dielectric materials. The epoxy discs were placed between two stainless-steel parallel plate electrodes with direct mechanical contact. The cell is connected to the Alpha-A analyzer with DETACHEM software. This configuration is suitable for low-loss dielectric materials and is fully compliant with Novocontrol's specifications for broadband dielectric analysis. All dielectric measurements were performed at room temperature (25–27 °C) under ambient laboratory atmosphere. Samples were placed inside the parallel-plate cell and allowed to equilibrate thermally for approximately 10 min before data acquisition then a constant AC excitation of 1 V_{rms} was applied to the samples over a frequency range of 10^{-1} – 10^6 Hz.

Breakdown strength

The AC breakdown strength of the epoxy Zn/Al-LDH nanocomposites was determined using (Breakdown Tester, Model Foster 60AF/2, Megger Ltd., Dover, UK) shown in Fig. 4. According to the procedure recommended by ASTM (D3755–14), a disk sample (5cm x 5cm) of 1 mm thickness was placed between two spherical copper electrodes and fully immersed in clean insulating oil within a standard oil-cell test fixture to suppress surface flashover. A 50 Hz sinusoidal voltage was applied and increased linearly at 500 V/s until dielectric failure occurred. Fifteen replicates per composition were tested to ensure statistical reliability. The breakdown data were analyzed using Weibull distribution to evaluate the reliability and dispersion of breakdown strength values across different filler loadings.



Fig. 4. (a) Megger Foster 60AF/2 Oil tester, (b) Test step.

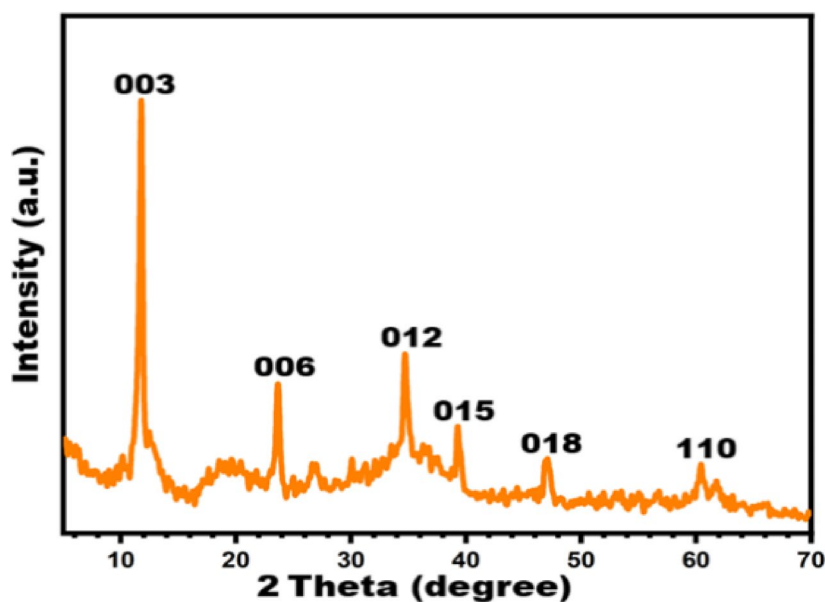


Fig. 5. XRD patterns for synthesized Zn-Al-CO₃ LDHs.

Results and discussion

Characterization of nanoparticles

To comprehensively elucidate the structural, morphological, and textural properties of the synthesized Zn/Al-layered double hydroxide (LDH) materials, a combination of advanced characterization techniques was employed, including X-ray diffraction (XRD), high-resolution transmission electron microscopy (HR-TEM) coupled with selected area electron diffraction (SAED), and nitrogen adsorption–desorption isotherm analysis.

XRD analysis was employed to investigate the crystalline phase composition and structural characteristics of the synthesized Zn/Al-layered double hydroxide (LDH). As depicted in Fig. 5, the diffraction patterns clearly indicate the formation of two distinct hexagonal phases, identified as Zn_{0.63}Al_{0.37}(OH)₂(CO₃)_{0.185}·xH₂O (PDF#00-048-1024) and Zn_{0.61}Al_{0.39}(OH)₂(CO₃)_{0.195}·xH₂O (PDF#00-048-1025). These phases exhibit well-defined basal and non-basal reflections at 2θ values of 11.76° (003), 23.57° (006), 34.69° (012), 39.23° (015), 47.07° (018), and 60.43° (110), corresponding to interlayer spacings (d-values) of 7.53871 Å, 3.76327 Å, 2.58342 Å, 2.33959 Å, 1.93069 Å, and 1.52867 Å, respectively. These reflections confirm the presence of a well-ordered layered structure, characteristic of LDH materials.

Quantitative analysis using Match! software (version 3.15) determined an average crystallite size of approximately 33.7 nm, indicative of nanocrystalline domains. The calculated crystallinity degree of 50.65% suggests a semi-ordered structure, which is often advantageous for applications of electrical insulation. Structurally, the Zn-Al-CO₃ LDHs consist of positively charged brucite-like layers, [M_{1-x}²⁺·M_x³⁺·(OH)₂]⁺X⁻,

composed of Zn^{2+} and Al^{3+} cations, balanced by interlayer carbonate anions (CO_3^{2-}) and water molecules^{14–16}. This lamellar architecture (Fig. 6) inherently restricts the mobility of free charge carriers, thereby contributing to low electrical conductivity, a desirable trait for electrical insulation applications¹⁷. Furthermore, the low crystallinity and nanoscale crystallite size imply a high density of grain boundaries and structural defects, which act as electron scattering centers, further impeding charge transport¹⁸. The incorporation of Al^{3+} ions enhance the dielectric strength and thermal stability of the material, both of which are critical parameters for effective electrical insulation¹⁹.

High-resolution transmission electron microscopy (HR-TEM) analysis reveals that the synthesized Zn-Al- CO_3 layered double hydroxide (LDH) nanoparticles exhibit a predominantly fibrous and rod-like morphology, with entangled structures that are uniformly distributed across the observed field. The particles display well-defined edges and consistent dispersion, indicating a controlled synthesis process that effectively regulates particle growth. The measured dimensions of these nanostructures are consistently below 100 nm, confirming their nanoscale nature and suggesting a high surface-to-volume ratio. This morphological feature is particularly advantageous for insulation applications, where enhanced surface area contributes to improved thermal and dielectric properties²⁰.

To further assess the structural order of the nanoparticles, selected area electron diffraction (SAED) was employed. The resulting SAED patterns exhibit concentric diffraction rings, a hallmark of polycrystalline materials. These rings correspond to various crystallographic planes, confirming the presence of multiple crystalline domains within the LDH structure^{21,22}. However, the relatively low intensity of the diffraction rings suggests that the material is not fully crystalline but rather exhibits a semi-crystalline nature. This intermediate crystallinity reflects a balance between ordered layer stacking and structural disorder; hence, the results obtained from HR-TEM/SAED techniques (Fig. 7) are in complete agreement with the XRD data.

The nitrogen adsorption/desorption isotherms and pore size distribution of Zn/Al- CO_3 LDH, as depicted in Fig. 8, were systematically analyzed using the BET and BJH models to evaluate its textural characteristics^{23,24}. The LDH exhibited a Type IV isotherm with an H3 hysteresis loop, in accordance with IUPAC classification, which is indicative of a mesoporous structure with slit-like pores typically associated with layered materials^{25–28}.

This observation is fully consistent with the BET-derived parameters listed in Table 2, where the material demonstrates a notably high specific surface area of $98.893 \text{ m}^2 \text{ g}^{-1}$ and a substantial total pore volume of $0.5279 \text{ cm}^3 \text{ g}^{-1}$, indicating extensive accessible porosity.

The BJH pore-size distribution, presented in the inset of Fig. 8a, further supports the mesoporous nature of the material. As detailed in Table 2, the pore network is centered around a dominant peak at 18.387 nm, with an average pore diameter of 18.738 nm and a median pore diameter of 20.227 nm, collectively reflecting a narrow and unimodal mesopore distribution. Moreover, t-plot analysis confirms the absence of microporosity, reinforcing that the synthesized LDH is governed entirely by mesoporous texturing.

Importantly, Fig. 8b presents a schematic model for slit-like pores, which conceptually illustrates the expected pore geometry derived from the adsorption data.

These structural features are particularly advantageous for electrical insulation applications. The high surface area facilitates uniform dispersion of LDH particles within polymer matrices, enhancing interfacial adhesion and reducing the likelihood of agglomeration, which is critical for maintaining consistent dielectric properties²⁹.

In addition, the mesoporous architecture may participate in charge-carrier moderation through increased interfacial area, although this effect likely acts in synergy with other mechanisms such as polarization at filler-matrix boundaries and improved structural ordering^{30–32}.

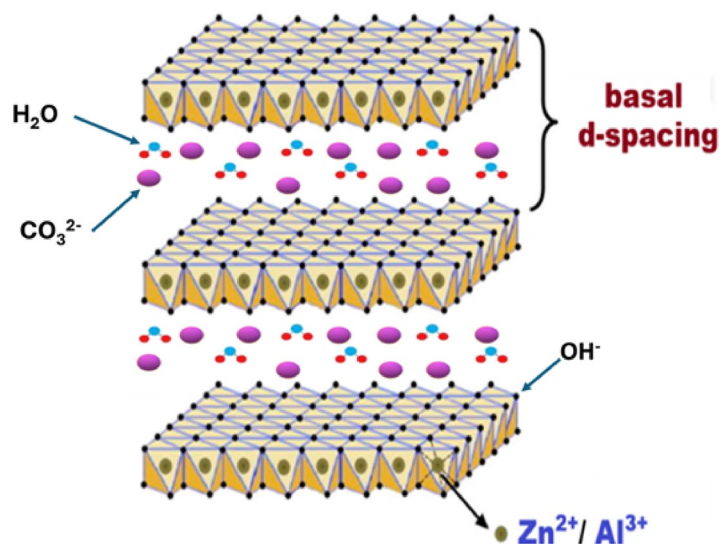


Fig. 6. Lamellar architecture and brucite-like layers of synthesized Zn-Al- CO_3 LDH.

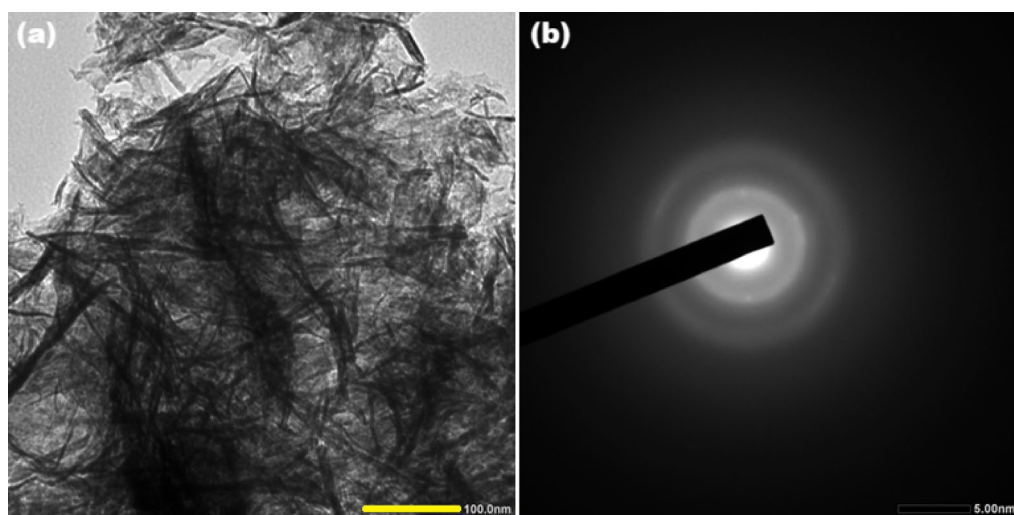


Fig. 7. (a) HR-TEM and (b) SAED of synthesized Zn-Al-CO₃ LDH.

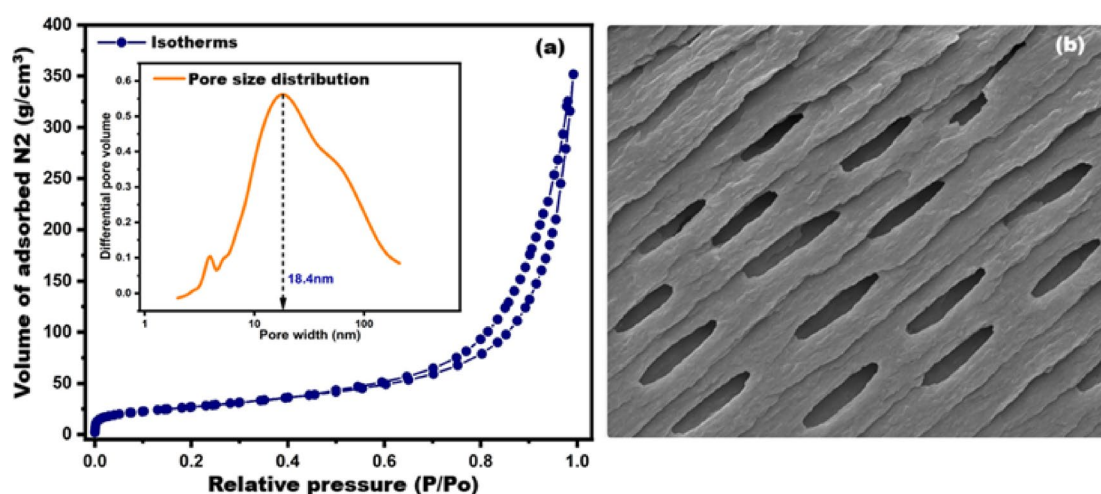


Fig. 8. (a) Isotherms/pore size distribution of synthesized LDH and (b) a model for slit-like pores.

Technique	Parameter	Value	Unit
BET	Specific surface area	98.893	m ² g ⁻¹
	Total pore volume	0.5279	cm ³ g ⁻¹
BJH	Peak pore diameter	18.387	nm
	Average pore diameter	18.738	nm
	Median pore diameter	20.227	nm

Table 2. BET, and BJH characterization results.

The substantial pore volume also enables the incorporation of functional additives, such as flame retardants or conductive suppressors, which can be tailored to enhance the thermal stability and multifunctionality of the insulation system³³. Overall, the textural characteristics of Zn/Al-CO₃ LDH contribute as part of a combined set of mechanisms that support dielectric enhancement and stability, rather than acting independently as the primary governing factor.

Characterization of epoxy nanocomposites

To thoroughly investigate the phase composition, surface morphology, and thermal stability of the synthesized LDH@epoxy nanocomposite, a suite of advanced characterization techniques was systematically employed.

These included X-ray diffraction (XRD) for identifying crystalline phases and structural integrity, scanning electron microscopy coupled with energy-dispersive X-ray spectroscopy (SEM/EDX) for detailed morphological and elemental analysis, and thermogravimetric analysis/differential scanning calorimetry (TGA/DSC) to assess thermal behavior, decomposition patterns, and heat flow characteristics. This multi-technique approach enabled a comprehensive understanding of the material's structural and functional properties, which are critical for evaluating its performance in insulation applications.

As illustrated in Fig. 9, the XRD analysis of pure epoxy (black curve) reveals two broad diffraction bands centered around $2\theta \approx 20^\circ$ and 44° , characteristic of its predominantly amorphous nature. These broad features reflect the disordered molecular arrangement and lack of long-range crystalline order, which is typical of cross-linked thermosetting polymer systems³⁴.

Upon incorporation of 5 wt% mesoporous Zn/Al-CO₃-LDH nanorods into the epoxy matrix, the XRD pattern of the LDH@epoxy composite (orange curve) exhibits significant structural changes. Notably, new diffraction peaks emerge at $2\theta \approx 11.47^\circ$, 19.23° , 20.69° , 22.37° , 31.21° , 34.53° , 39.35° , and 44.31° , which are absent in the pure epoxy pattern. These peaks indicate the presence of crystalline LDH (PDF#00-048-1024) domains and suggest strong interfacial interactions between the LDH and epoxy matrix, likely due to polymer chain intercalation or chemical bonding that modifies the lattice spacing³⁵.

The appearance of sharper and more intense peaks in the composite indicates an increase in structural ordering from 21.08% to 28.92%, as computed automatically through quantitative pattern analysis using Match! software (version 3.15).

Such modifications may also reflect internal stress or strain within the composite³⁶, further confirming the successful integration of LDH. These structural enhancements are crucial for electrical insulation applications, as they contribute to improved dielectric behavior, reduced charge mobility through effective trapping, and greater thermal stability. Overall, the XRD results substantiate the reinforcing role of LDH in epoxy composites and underscore its potential for advanced insulation systems.

Thermogravimetric analysis (TGA) and derivative thermogravimetry (DTG) profiles presented in Fig. 10a, b reveal distinct thermal behaviors between the neat epoxy and the epoxy nanocomposite containing 5 wt% Zn/Al-LDH. The neat epoxy (Fig. 10a) exhibits thermal stability up to approximately 300 °C, beyond which significant degradation initiates between 346–370 °C. The DTG curve shows a sharp peak at 375 °C, indicating the maximum rate of mass loss, with the primary decomposition occurring between 370–450 °C and leaving a residual char of ~14% at 700 °C.

In contrast, the LDH-modified epoxy (Fig. 10b) exhibits an early mass-loss event at ~172 °C, mainly associated with the release of physically adsorbed or interlayer water and a minor surface dehydroxylation of weakly bound hydroxyl groups. This behavior agrees with previous reports on LDH-containing systems, where an initial mass loss (50–250 °C) corresponds to dehydration and partial decomposition of hydroxide phases^{15,16}. Despite this initial event, the main decomposition onset (~338 °C) and peak degradation temperature (375 °C) remain comparable to the neat epoxy. However, the final char residue increases to ~17.1%, signifying enhanced thermal stability. This improvement is consistent with the barrier effect and char-promoting properties of LDH nanofillers, which contribute to the formation of a more thermally resilient composite structure.

Differential scanning calorimetry (DSC) is a standard thermal analysis for polymer characterization that records heat flow to/from a specimen. At the same time, its temperature is programmed under an inert or reactive purge. The technique resolves exothermic and endothermic events; the associated transition temperatures (e.g., glass transition, melting, evaporation, or decomposition). For amorphous polymers, the glass transition

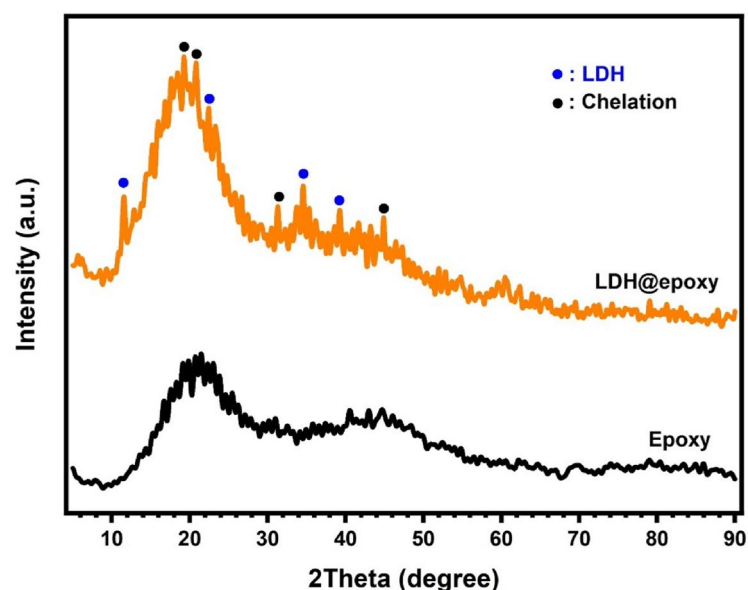


Fig. 9. XRD patterns of pure epoxy and LDH@epoxy.

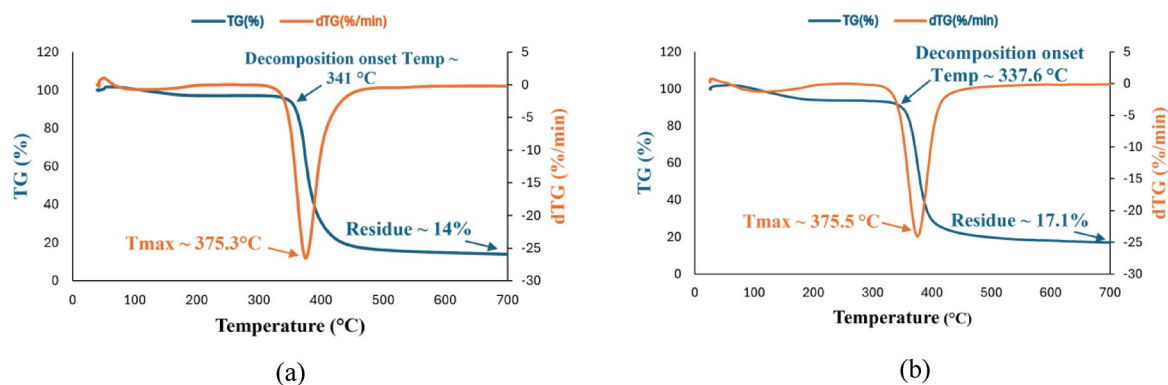


Fig. 10. (a) TGA for pure epoxy sample, (b) TGA for epoxy Zn/Al-LDH (5%) nanocomposite.

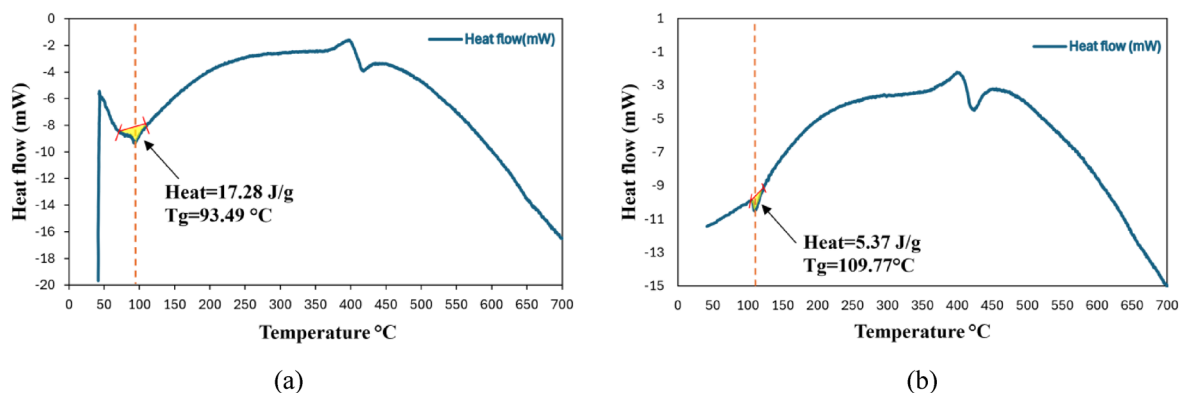


Fig. 11. (a) DSC test for pure epoxy sample, (b) DSC test for epoxy Zn/Al-LDH (5%) nanocomposite.

temperature (T_g) marks the change from glassy to rubbery/viscous behavior and is accompanied by a heat-capacity step (ΔC_p). In this work, the same DSC protocol will be applied to the neat epoxy and to the 5% Zn/Al-LDH/epoxy nanocomposite to compare T_g and ΔC_p . Differential scanning calorimetry revealed a clear shift in the glass transition behavior upon the incorporation of Zn/Al-LDH nanofillers. For the neat epoxy in Fig. 11a, the glass transition temperature (T_g) was identified at 93.5 °C, accompanied by a relatively large enthalpic relaxation of approximately 17.3 J/g. This combination reflects the high mobility of polymer chain segments and the limited constraints within the pure epoxy network. In contrast, the nanocomposite containing 5 wt% Zn/Al-LDH in Fig. 11b exhibited a distinctly higher T_g of 109.8 °C, together with a markedly lower relaxation enthalpy of only 5.4 J/g. The upward shift in T_g indicates that the nanofiller restricts the segmental dynamics of the epoxy chains, consistent with enhanced interfacial interactions and increased effective crosslink density^{37–39}.

At the same time, the pronounced reduction in ΔH implies that fewer cooperative chain motions occur during the transition, as the LDH platelets act as barriers to chain mobility and promote a more rigid network structure^{37–39}. These findings corroborate the role of layered double hydroxides in improving the thermal stability and dimensional integrity of epoxy matrices under heating.

According to the IEC 62271-1 standard, the maximum allowable operating temperatures are 105 °C for the conductor that is in contact with the spacer material⁴⁰. In this study, the neat epoxy exhibited a T_g of ~93.5 °C, which falls below this threshold. However, the incorporation of 5 wt% Zn/Al-LDH in epoxy successfully shifted T_g to ~109.8 °C, surpassing the IEC guideline.

Figure 12 presents SEM/EDX micrographs of the neat epoxy (Fig. 12a) and LDH@epoxy (Fig. 12b). In the neat epoxy, the surface appears relatively smooth and homogeneous, with no distinct inorganic features or secondary phases. Only a few scattered bright spots can be observed, which are most likely attributed to preparation artefacts or surface debris rather than actual structural components. Overall, the micrograph confirms the purity of the epoxy matrix and provides a reliable baseline for comparison with the nanocomposite⁴¹. In contrast, the micrograph of LDH@epoxy reveals a markedly different surface morphology. Bright regions and irregularly shaped clusters are clearly distributed across the matrix, corresponding to the presence of LDH nanoparticles. Their enhanced contrast originates from the higher atomic number of Zn and Al compared to the carbon-rich epoxy background, resulting in stronger electron scattering. The occurrence of agglomerates is a common feature in polymer–nanofiller systems, arising from the high surface energy of nanoparticles. Nevertheless, the overall distribution of bright particles across the surface confirms the successful incorporation of the nanofiller into the epoxy. Energy-dispersive X-ray spectroscopy (EDX) was used to verify the elemental composition of the

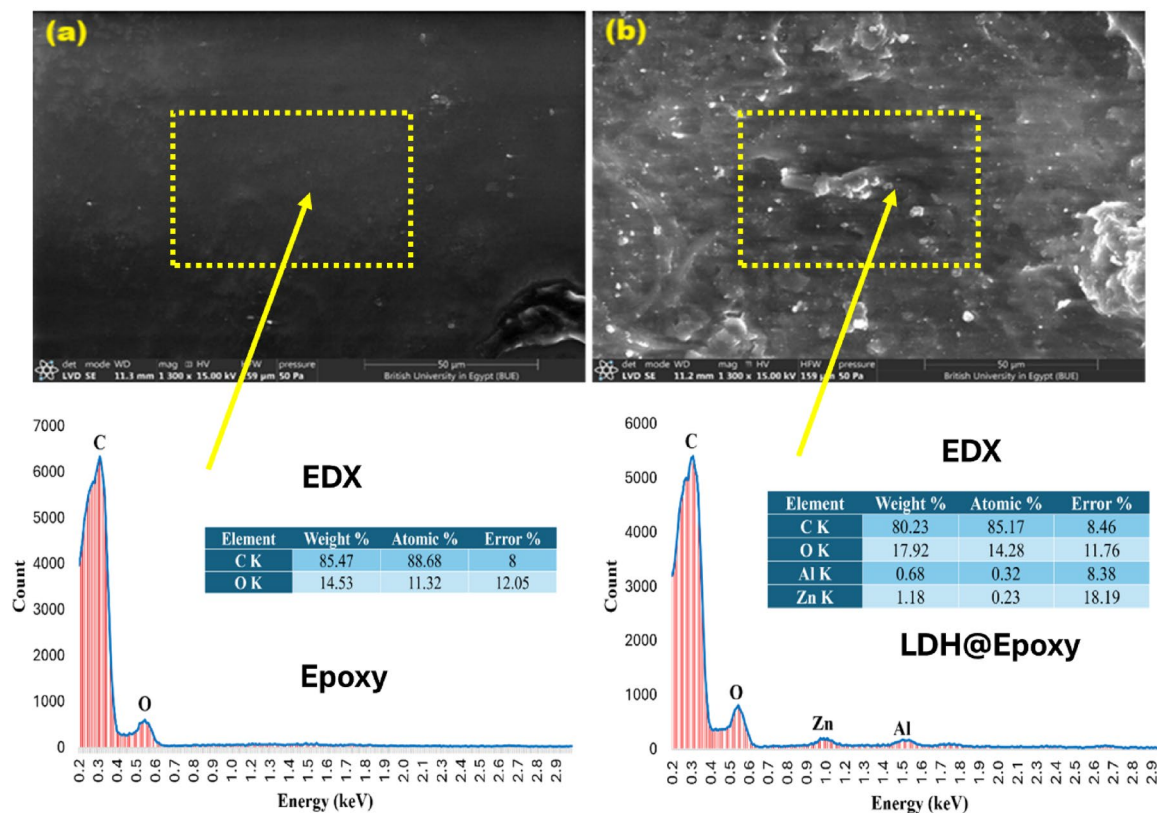


Fig. 12. SEM/EDX images of (a) pure epoxy and (b) LDH@epoxy.

neat epoxy and the Epoxy/Zn–Al (LDH) composite, to check for contaminants, and to provide semi-quantitative weight/atomic percentages with instrument-reported errors⁴². The EDX spectrum for the neat epoxy shows only the polymeric constituents, with a dominant C K α peak at ~0.28 keV and a weaker O K α peak at ~0.53 keV; the semi-quantitative analysis gives C = 85.47 wt.% (88.68 at%) and O = 14.53 wt.% (11.32 at%), consistent with an organic matrix. After adding the Zn–Al LDH, two additional signals appear at the expected positions of Zn L (~1.01 keV) and Al K α (~1.49 keV), confirming successful incorporation of the LDH-nanorod. The matrix still dominates, but the carbon fraction decreases to 80.23 wt%, accompanied by a rise in oxygen to 17.92 wt%, which is consistent with the hydroxyl-rich LDH surface. Minor amounts of Zn = 1.18 wt.% (0.23 at%) and Al = 0.68 wt.% (0.32 at%) are detected; the larger uncertainty on Zn (18.19%) reflects its low concentration and the low-energy region's higher absorption. No extraneous elements were observed above background, indicating a clean composite and validating the presence of Zn/Al-LDH within the epoxy.

The variations in C and O content between the neat epoxy and LDH@epoxy samples are fully consistent with the expected incorporation of the oxygen-rich LDH filler into the polymer matrix. The slight decrease in carbon (from 85.47 to 80.23 wt%) and corresponding increase in oxygen (from 14.53 to 17.92 wt%) reflect the presence of hydroxylated Zn–Al–LDH nanosheets, which contain abundant OH groups and metal oxygen bonds.

Dielectric performance of epoxy nanocomposites

The subsequent section evaluates three essential dielectric characteristics of epoxy composites incorporating four varying concentrations of Zn/Al-LDH nanoparticles: relative permittivity, loss tangent ($\tan \delta$), and electrical conductivity.

Relative permittivity

The frequency-dependent behavior of the relative permittivity (ϵ') for epoxy nanocomposites filled with various weight percentages of Zn/Al-LDH exhibits a non-monotonic response at any frequency point, reflecting the complex interplay between interfacial polarization, filler dispersion, polymer chain dynamics, and nano-interfacial structure formation. Conversely, as shown in Fig. 13, for any single wt.% ϵ' exhibits a typical monotonic decreasing trend with increasing frequency.

At low frequencies, the dipolar entities within the polymer matrix have sufficient time to orient themselves in response to the alternating electric field. This alignment with the changing field polarity leads to higher values of the relative permittivity. However, as the frequency increases, the dipoles can no longer follow the rapid field reversals, causing a gradual loss of polarization coherence and consequently a decrease in the relative permittivity with frequency.

However, a minor contribution from interfacial (Maxwell–Wagner–Sillars) polarization can still be expected at low frequencies, where charge accumulation at filler–matrix interfaces cannot be neglected. This interpretation

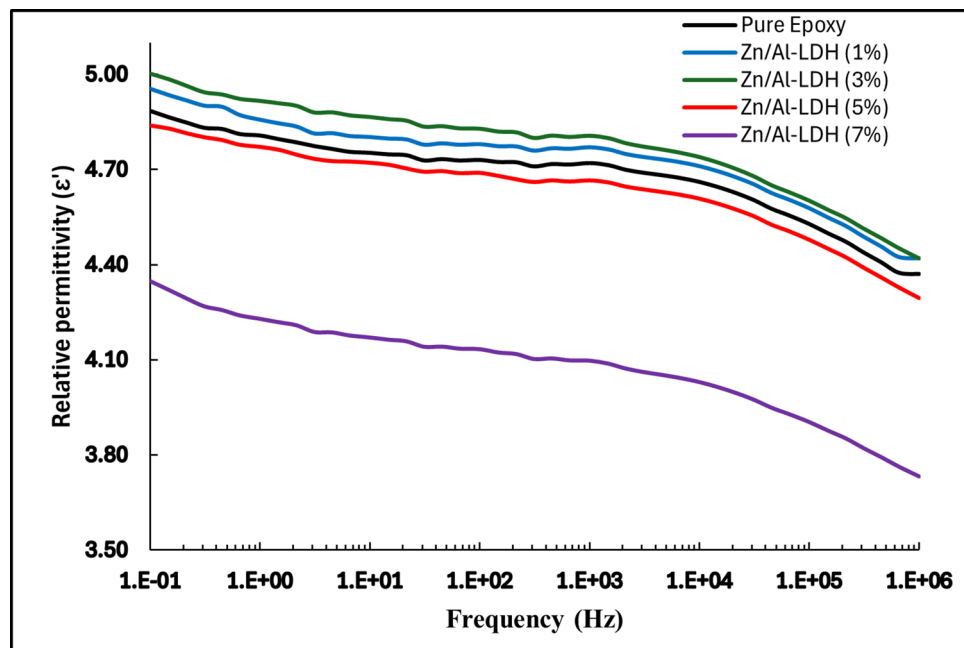


Fig. 13. Variation of relative permittivity with frequency.

is consistent with the model proposed by Xia et al. which demonstrated an inverse relationship between the interfacial (Maxwell–Wagner–Sillars) relative permittivity and frequency, arising from charge accumulation at the filler–matrix boundaries in heterogeneous polymer nanocomposites⁴³.

The effect of filler concentration on ϵ' reveals a nuanced dielectric response. At low concentrations, 1 and 3 wt.% of Zn/Al-LDH, the permittivity slightly increased compared to the neat epoxy, which can be attributed to improved dispersion and the formation of interfacial regions that contribute positively to the polarization process. These interfacial regions act as dipole-rich zones, allowing for additional alignment with the applied electric field and thereby increasing the net dielectric storage capability⁴.

At 5 wt.%, a noticeable decline in permittivity is observed. This drop is primarily associated with the formation of immobilized nanolayers, which are rigid polymer regions surrounding the LDH particles. These layers suppress the mobility of polymer chains and inhibit the orientation of nearby dipoles, effectively reducing the material's ability to store electric energy. The presence of such immobilized zones marks the onset of interfacial rigidity, which counteracts the benefits of polarization introduced at lower concentrations^{4,7}. Similar interfacial immobilization effects have been reported in LDH/polymer nanocomposites, where reduced segmental dynamics near LDH layers lead to lower dielectric response⁴⁴.

At 7 wt.%, the permittivity undergoes a significant reduction, becoming markedly lower than that of the neat epoxy. This decline is indicative of extensive filler agglomeration and the dominance of immobilized nanolayer structures. To provide a more detailed qualitative and quantitative description of the agglomeration behavior at 7 wt.%, a SEM micrograph was conducted as shown in Fig. 14 clearly reveals the presence of dense agglomerates with irregular morphology and poor interparticle dispersion. The observed clusters exhibit sizes ranging from approximately 1 to 6 μm , occupying nearly 30% of the field of view (Fig. 14).

The observed agglomeration reduces the effective interfacial surface area, leading to non-uniform filler distribution and dielectric inhomogeneity. Furthermore, the high filler content amplifies the extent and continuity of the immobilized regions, thereby restricting the dipolar response to larger volumes of the matrix. Consequently, the dielectric contribution from both the matrix and the filler becomes severely diminished⁷.

The intrinsic properties of the LDH structure, specifically those of Zn/Al-LDH, play a central role in shaping this dielectric behavior. The lamellar and ionic nature of LDH particles make them inherently polar, favoring interfacial polarization at moderate concentrations. However, their hydrophilic surfaces and tendency to form hydrogen bonds with the polymer matrix promote the formation of tightly bound immobilized layers. This unique interfacial chemistry, while initially beneficial for polarization, becomes detrimental at higher loadings due to excessive constraint of molecular mobility. Unlike spherical fillers, LDHs introduce anisotropic field distributions and stronger electrostatic interactions at the interface. These characteristics enhance dipole immobilization and facilitate the rapid development of rigid interfacial zones, especially as particle proximity increases⁹.

Tan(δ)

The dielectric loss tangent, $\tan(\delta)$, is a critical parameter that quantifies the phase lag between electric field and polarization response, effectively measuring the proportion of energy dissipated as heat in a dielectric material. For epoxy nanocomposites containing various loadings of Zn/Al layered double hydroxide (LDH), the frequency-dependent behavior of $\tan(\delta)$ reveals essential information regarding dielectric relaxation, interfacial

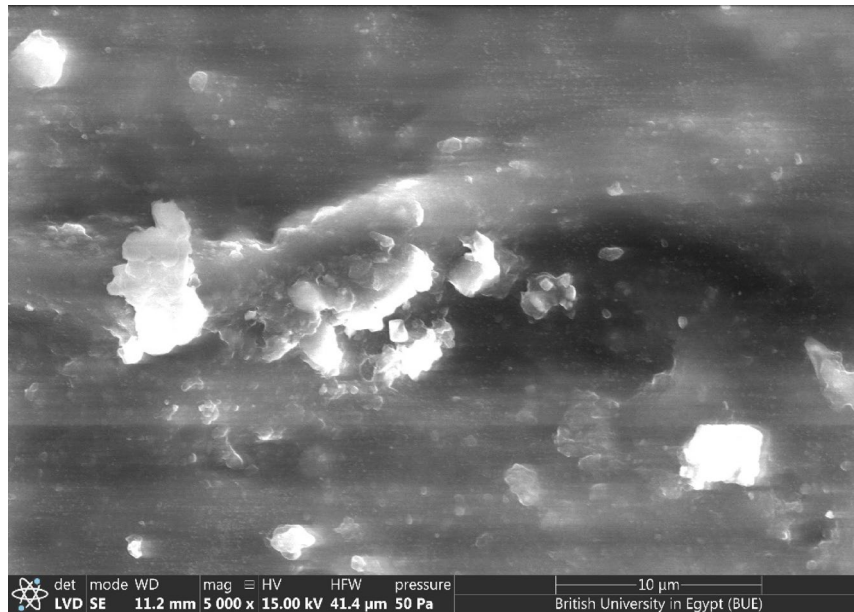


Fig. 14. SEM micrograph for 7% Zn/Al-LDH epoxy sample.

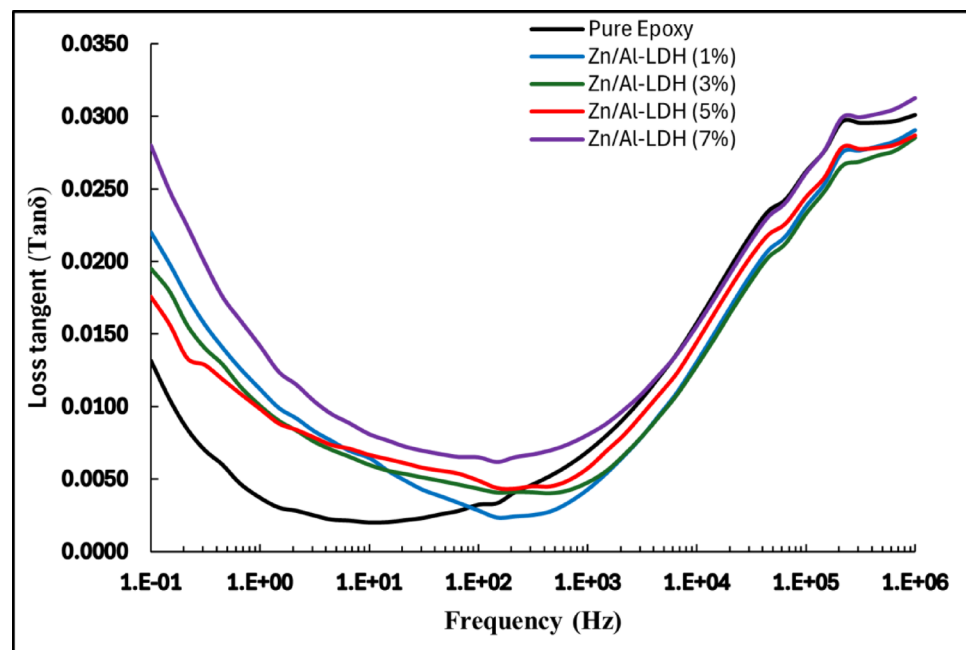


Fig. 15. Variation of tan delta with frequency.

phenomena, and the balance between permittivity and energy loss. Across the frequency range, as illustrated in Fig. 15, all samples demonstrate a U-shaped $\tan(\delta)$ curve, with higher values at both low and high frequency extremes and a distinct minimum in the intermediate range (approximately $10\text{--}10^3$ Hz).

At very low frequencies (below 1 Hz), dielectric materials, especially polymer nanocomposites, exhibit a significant increase in dielectric loss ($\tan \delta$). This behavior is primarily attributed to three mechanisms: conduction loss due to the drift of free or impurity charges under the slow-varying field; interfacial polarization (Maxwell–Wagner–Sillars effect) arising from permittivity and conductivity mismatch between filler and matrix, which leads to charge accumulation at interfaces; and space charge relaxation, where deeply trapped charges gradually respond to the applied field. These combined effects result in higher energy dissipation and elevated loss factors in the low-frequency regime⁴⁵.

This characteristic behavior reflects the combined effects of interfacial polarization at low frequencies and the losses due to immobilized layers at higher frequencies. The intermediate region corresponds to frequencies

where polarization mechanisms are most effectively aligned with the applied field, leading to lower loss tangent values.

Adding the Zn/Al-LDH nanofiller with all the weights increases the value of $\tan(\delta)$ in the region of low frequency below 200 Hz, where the interfacial polarization is dominant. Additionally, it is noticeable that the rate at which the composite eliminates this effect increases as the weight of the nanofiller decreases. On the other hand, adding the nanofillers shows better performance in the high-frequency region, where 1, 3 and 5 wt.% show lower losses than that of the pure epoxy⁴.

The addition of a vertical reference at 50 Hz, corresponding to the standard power frequency in AC electrical systems, provides practical context to the dielectric loss analysis. The $\tan(\delta)$ values at this frequency, extracted for each filler concentration, show only minor variations across all samples. While slight increases are observed with higher Zn/Al content, particularly at 5 wt.% and 7 wt.%, the changes are modest and well within acceptable design tolerances for high-voltage insulation materials.

Conductivity

Electrical conductivity is a critical parameter in assessing the insulation capability of polymer-based materials. For high-voltage applications, particularly under alternating fields or fast switching conditions, the material must exhibit very low conductivity over a broad frequency range to minimize energy losses and prevent current leakage. Frequency-dependent conductivity analysis is thus a powerful diagnostic tool to evaluate the dielectric integrity of epoxy-based nanocomposites subjected to such operational stresses.

The AC conductivity can be extracted from the imaginary part of the complex permittivity using the Eq. (1):

$$\sigma'(\omega) = \omega \varepsilon_0 \varepsilon''(\omega) \quad (1)$$

where: σ' is the real part of conductivity [S/cm], ε_0 is the vacuum permittivity (8.854×10^{-12} F/m), ε'' is the imaginary part of permittivity, and $\omega = 2\pi f$ is the angular frequency.

Figure 16 illustrates the frequency dependence of the real part of AC conductivity (σ') for the pure epoxy and Zn/Al-LDH epoxy nanocomposites at various filler loadings (1–7 wt.%), plotted on a log–log scale.

In the low-frequency region approximately up to 100 Hz, the conductivity remains nearly constant, displaying a flat plateau. This behavior corresponds to the dominance of DC conductivity (σ_{DC}), which in this case is extremely low, ranging from 10^{-15} to 10^{-13} S/cm. Such minimal conductivity ensures that the composite behaves as a perfect insulator under static or slowly varying fields, a highly desirable trait for HV insulation systems⁴.

Comparing the different loadings, the DC conductivity at low and intermediate frequencies slightly increases up to 3 wt.%, attributed to the formation of additional charge-transfer paths and enhanced interfacial polarization. Beyond this concentration, σ' decreases, particularly for the 7 wt.% sample, which exhibits the lowest conductivity across the whole frequency range. This reduction is linked to agglomeration of LDH nanorods, which disrupts the homogeneity of the matrix and restricts carrier motion.

In the mid and high frequency region an onset of dispersion occurs at this region marks the transition from frequency-independent to frequency-dependent behavior. σ' shows a progressive rise for all samples, consistent with Jonscher's universal power law $\sigma'(\omega) = \sigma_{DC} + A\omega^n$. This behavior indicates that conduction is mainly governed by hopping or tunneling of charge carriers between localized states within the polymer–filler network⁴.

Importantly, even in this regime, the conductivity remains within a safe window (typically below 10^{-8} S/cm), maintaining excellent insulation behavior.

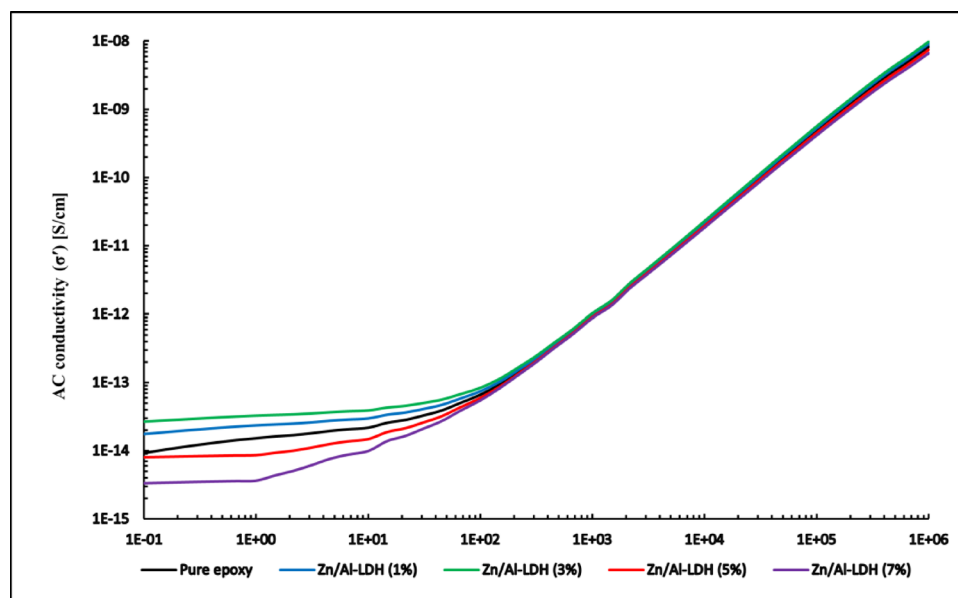


Fig. 16. Variation of conductivity with frequency.

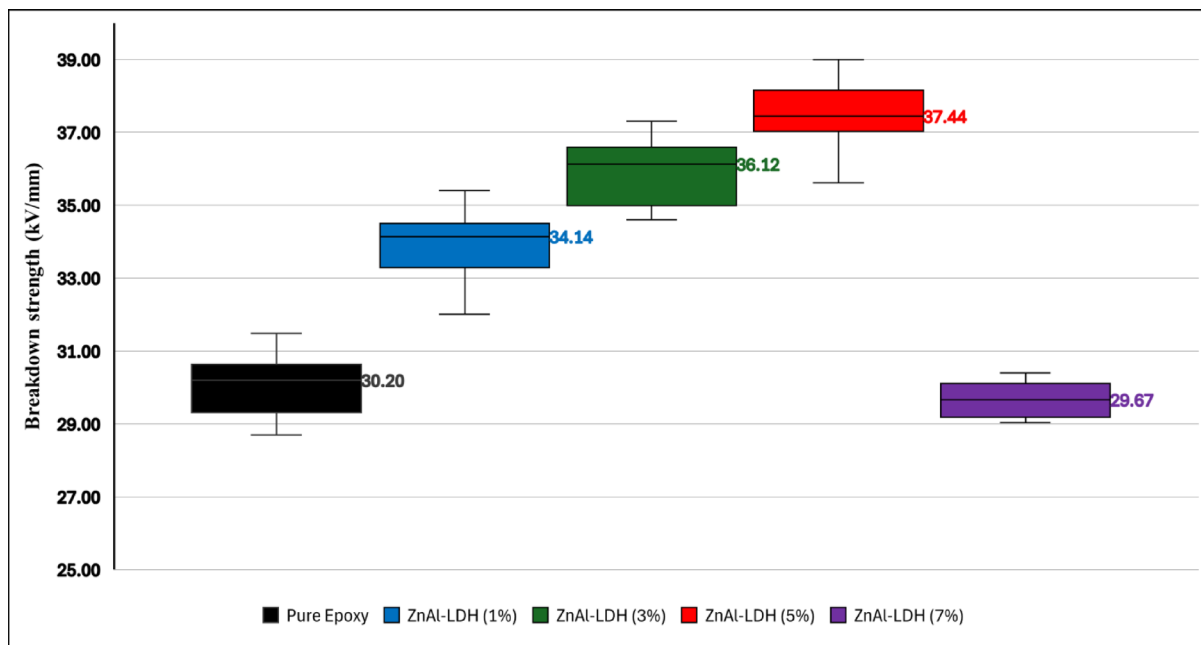


Fig. 17. A boxplot visualizes the distribution and identifies outliers in the BDS test.

Material	Min (kV/mm)	Max (kV/mm)	Mean (kV/mm)	Std Deviation (kV/mm)	Coefficient of Variation (%)
Pure Epoxy	28.7	31.5	30.08	0.91	2.03
Zn/Al-LDH (1%)	32	35.4	33.9	0.88	2.61
Zn/Al-LDH (3%)	34.6	37.3	36.06	0.9	2.5
Zn/Al-LDH (5%)	35.6	39	37.42	0.99	2.64
Zn/Al-LDH (7%)	29	30.4	29.68	0.49	3.66

Table 3. Basic statistics for the BDS test.

The overall conductivity profile strongly supports the classification of the tested epoxy nanocomposites as high-performance insulating materials. The minimal σ_{DC} which covers the operating 50Hz frequency in GIS systems, and safe high-frequency behavior corresponding to overvoltage frequencies, all contribute to the material's reliability in high-voltage environments. These findings are highly encouraging for deployment in GIS, GITL, and other advanced insulation systems requiring stability across wide frequency ranges.

Breakdown strength performance of epoxy nanocomposites

Epoxy specimens were evaluated in their unfilled (pure) state as well as with Zn/Al-LDH nanofillers at loadings of 1 wt.%, 3 wt.%, 5 wt.%, and 7 wt.%. For each formulation, 15 individual samples were tested. The boxplot shown in Fig. 17 visualizes the distribution of breakdown strength values and clearly indicates the median. Outliers were identified according to Tukey's $1.5 \times IQR$ criterion, where the interquartile range (IQR) represents the difference between the third (Q3) and first (Q1) quartiles. According to this criterion, no measured value was found to be an outlier.

The statistical summary in Table 3 reveals a nonlinear enhancement in BDS with increasing Zn/Al concentration. Specifically, the neat epoxy exhibited a mean value of 30.08 kV/mm with a standard deviation of 0.91. The incorporation of 1 wt.% Zn/Al increased the mean BDS to 33.90 kV/mm, and the addition of 3 wt.% Zn/Al further improved to 36.06 kV/mm. The maximum BDS was observed at 5 wt.%, reaching 37.42 kV/mm, beyond which a substantial decline occurred at 7 wt.%, falling back to 29.68 kV/mm, which is even lower than that of the neat epoxy. This trend suggests that an optimum nanofiller loading of between 3 and 5 wt.% maximizes dielectric strength.

The coefficient of variation (CV) supports the same conclusion. The 5 wt.% sample not only had the highest BDS mean but also maintained a low CV of 2.64%, indicating highly stable and reproducible breakdown behavior. The observed behavior can be rationalized in terms of interfacial polarization, filler dispersion quality, and immobilized interfacial regions, consistent with the permittivity data. At low filler concentrations (1–3 wt.%), the improved BDS is attributed to the formation of well-dispersed interfacial zones between the Zn/Al-LDH particles and the polymer matrix. These regions enhanced dielectric polarization, suppressed local electric field intensities, and introduced charge trapping sites at the polymer filler interfaces, which capture injected charges and disrupt the continuous streamer channels responsible for breakdown propagation.

This interpretation is supported by the slight increase in ϵ' at 3 wt.% and the moderate $\tan(\delta)$ values, indicating efficient energy storage with minimal dielectric loss.

At 5 wt.% Zn/Al, the composite appears to reach an optimal balance. The permittivity analysis confirms that while ϵ' slightly decreases, the slight suppression in ϵ'' and $\tan(\delta)$ at this concentration suggests that the immobilized nanolayers formed around the fillers act as deep charge traps, stabilizing the internal field distribution and boosting breakdown resistance.

Moreover, the inherent nature of Zn/Al as a layered double hydroxide (LDH) further amplifies these effects. The lamellar structure of LDHs provides a high interfacial area, facilitating strong hydrogen bonding with the epoxy matrix and promoting the formation of immobilized interfacial nanolayers. These features not only enhance interfacial polarization at moderate concentrations but also increase the interfacial trap density and charge retention capacity⁹.

Interfacial polarization facilitates charge trapping and mitigating local electric stress by redistributing the electric field and creating localized regions of charge accumulation at the filler matrix interface. At optimized filler loadings, this reduces field concentration and delays breakdown. However, excessive interfacial polarization due to agglomeration or high filler content can instead lead to localized field intensification.

The histogram plots presented in Fig. 18 provide a clear statistical visualization of the breakdown strength (BDS) measurements for all epoxy and Zn/Al-LDH nanocomposite formulations. These distributions offer critical insights into the repeatability, stability, and intrinsic variability of the experimental data, thereby supporting the validity of the subsequent Weibull reliability analysis.

Across all samples, the histograms exhibit well-defined, unimodal distributions, indicating that the BDS values cluster around a dominant central tendency with limited scattering. This behaviour reflects a high degree of measurement consistency and suggests that the specimens within each formulation respond in a statistically uniform manner. The frequency profiles also reveal the absence of extreme outliers or irregular secondary peaks, demonstrating that the fabrication process yielded samples with reproducible breakdown behaviour. Such

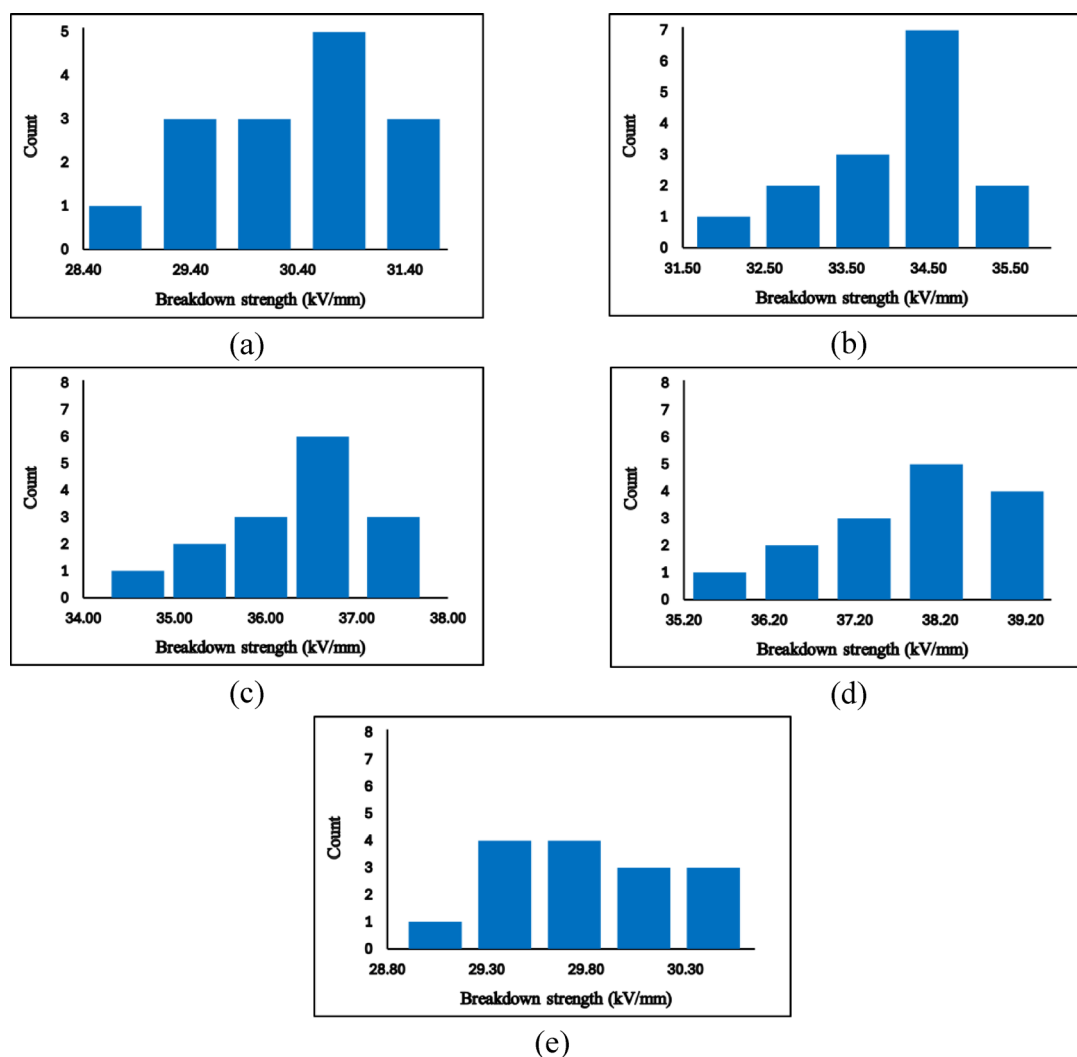


Fig. 18. A histogram shows the frequency distribution of BDS values. (a) pure epoxy, (b) Zn/Al (1%), (c) Zn/Al (3%), (d) Zn/Al (5%), and (e) Zn/Al (7%).

well-behaved distributions are essential in high-voltage dielectric studies, as they confirm that the observed improvements are intrinsic to the material system rather than artefacts of random experimental fluctuation.

Furthermore, the compactness of the histograms for the optimal filler loadings implies a reduction in stochastic variability typically associated with microstructural defects and localized weak points. This observation reinforces the hypothesis that the incorporation of Zn/Al-LDH at moderate concentrations promotes a more uniform dispersion and contributes to a more robust dielectric network capable of sustaining higher electric fields before failure.

Weibull distribution

Weibull analysis plays a crucial role in interpreting dielectric breakdown strength (BDS) data, particularly for polymeric insulation materials. It offers a deeper understanding of the distribution of breakdown events: the shape parameter (β) reflects the scatter of data, indicating the uniformity and consistency of failure. In contrast, the scale parameter (α) provides a measure of the characteristic breakdown strength at which 63.2% of the specimens are expected to fail.

The two-parameter Weibull cumulative distribution function is given by the Eq. (2):

$$f(x) = 1 - \exp \left[- \left(\frac{x}{\alpha} \right)^\beta \right] \quad (2)$$

where: $F(x)$ is the cumulative probability of failure at stress level x , α is the scale parameter which describes the breakdown strength at which 63.2% of samples are expected to fail, and β is the shape parameter which is a dimensionless parameter indicating the dispersion and failure mode.

To linearize the equation and enable graphical interpretation, the double logarithmic form is often used:

$$\ln \left[-\ln \left(1 - f(x) \right) \right] = \beta \ln (x) - \beta \ln (\alpha) \quad (3)$$

$$y = \beta \ln (x) - \beta \ln (\alpha) \quad (4)$$

This transformation allows for a straight-line fit on a plot of $\ln(x)$ versus $\ln [-\ln(1-F)]$, where the slope represents β and the intercept is related to $-\beta \ln(\alpha)$. To apply the two-parameter Weibull distribution to the breakdown strength data, the measured values are first arranged in ascending order. The cumulative probability of failure for each ranked value is then estimated using Benard's approximation formula (5), then by plotting the double logarithmic form (3), a straight line is obtained whose slope represents the shape parameter β , while the scale parameter α is derived from the intercept $-\beta \ln(\alpha)$ as shown in Eq. (4):

$$f(x_i) = \frac{i - 0.3}{n + 0.4} \quad (5)$$

where: i is the rank of the value x_i from 1 to n , and n is the total number of data points.

To assess how well the Weibull curve fits the actual data points, the coefficient of determination R^2 is calculated for each data set. The R^2 values obtained for all samples fall within or above the generally accepted threshold for good statistical fit (≥ 0.90), confirming the suitability of the Weibull model in representing the breakdown behavior. All formulations exhibited strong linearity except for the 7 wt.% Zn/Al-LDH sample, which showed a noticeably lower R^2 value (0.877), likely due to nanofiller agglomeration and increased variability in dielectric performance.

Additionally, the summary of the Weibull parameters in Table 4 indicates that the addition of Zn/Al nanofillers yields a notable enhancement in dielectric performance, particularly at a 5 wt% concentration. The scale parameter α increased significantly from its baseline value in pure epoxy, indicating that most breakdown events in the nanocomposite occurred at higher electric field levels. This is consistent with the experimental observation of an improvement in dielectric strength. Similarly, the shape parameter β increased with the addition of 1%, 3%, and 5% Zn/Al, reflecting reduced variability and more homogeneous failure behavior, likely due to better field distribution and interface interaction.

However, at 7 wt.%, α is declined, signaling a deterioration in insulation quality. This behavior is attributed to the possible agglomeration of excess nanofiller particles, which may introduce local field enhancements and micro voids, acting as premature breakdown sites. This explanation is supported by the earlier permittivity analysis, which showed signs of interfacial polarization saturation and increased dielectric loss at higher concentrations, indicating a limit to the beneficial role of filler loading.

Material	R^2	α (kV/mm)	β
Pure Epoxy	0.9292	30.5	39.23
Zn/Al-LDH (1%)	0.972	34.31	46.26
Zn/Al-LDH (3%)	0.92	36.48	47.34
Zn/Al-LDH (5%)	0.9632	37.87	45.75
Zn/Al-LDH (7%)	0.877	29.91	69.77

Table 4. Weibull parameters of all data sets.

The high shape parameter value β should not be interpreted as improved reliability or superior insulation performance. Instead, it reflects the fact that, for the 7 wt.% composite, almost all specimens fail within a very narrow low-field range (29–30.4 kV/mm), as also seen from the basic statistics in Table 3 and the histogram in Fig. 18.

The logarithmic Weibull plot depicted in Fig. 19, confirms the model's applicability, showing a clear linear relationship across all formulations. The steepest slope and furthest rightward shift were observed at 5 wt.%, corroborating the superior performance and reliability at this loading. Meanwhile, the cumulative probability plot illustrated the distribution of breakdown events, and the horizontal α -line ($F = 63.2\%$) allowed direct comparison of characteristic strength across all samples. The gradual shift of the α -intercept toward higher voltages, up to 5 wt.%, and its retreat at 7 wt.%, visually support the statistical trends.

Another fundamental aspect that can be obtained from Weibull analysis is the reliability curve, which can be used in evaluating the performance and consistency of insulating materials under high-voltage stress. While traditional metrics such as the mean breakdown strength provide insight into the average performance, they fail to capture the statistical probability of failure at specific stress levels. This is where Weibull-based reliability assessment becomes essential, as it offers a more robust evaluation by considering both the strength distribution and the associated failure probabilities.

The equation defines the reliability function $R(x)$ for a Weibull-distributed variable (6):

$$R_{(x)} = \exp \left[- \left(\frac{x}{\beta} \right)^\alpha \right] \quad (6)$$

where: $R_{(x)}$ is the reliability at stress x .

The Weibull reliability curves are presented in Fig. 20 For all tested compositions. These curves represent the probability that each sample will withstand a given stress without breaking down. The results clearly show that adding Zn/Al-LDH nanofillers enhances reliability across the breakdown strength range. The 3 wt.% and 5 wt.% samples demonstrated the most favorable profiles, shifting the curves toward higher field values and indicating improved dielectric performance. In contrast, the 7 wt.% sample exhibited reduced reliability, likely due to nanoparticle agglomeration and interfacial degradation, which introduced local defects and field concentration points.

Conclusion

This work investigated the potential of Zn/Al layered double hydroxide (LDH) nanorods as functional fillers to enhance the dielectric and thermal performance of epoxy resin, aiming at their utilization in Gas-Insulated Switchgear (GIS) and Transmission Line (GITL) spacer applications.

A comprehensive experimental approach was adopted: the LDH nanofillers were synthesized, structurally characterized, and incorporated into epoxy at different loadings (1, 3, 5, and 7 wt.%). The resulting nanocomposites were then systematically evaluated through dielectric spectroscopy, breakdown strength testing, thermal analysis, and microstructural characterization. The key findings can be summarized as follows:

1. Zn/Al-LDH nanoparticles exhibited a nanocrystalline, semi-ordered layered structure with surface area $\sim 98.9 \text{ m}^2/\text{g}$. Also, the mesoporous architecture with an average pore diameter of $\sim 18.7 \text{ nm}$ provided

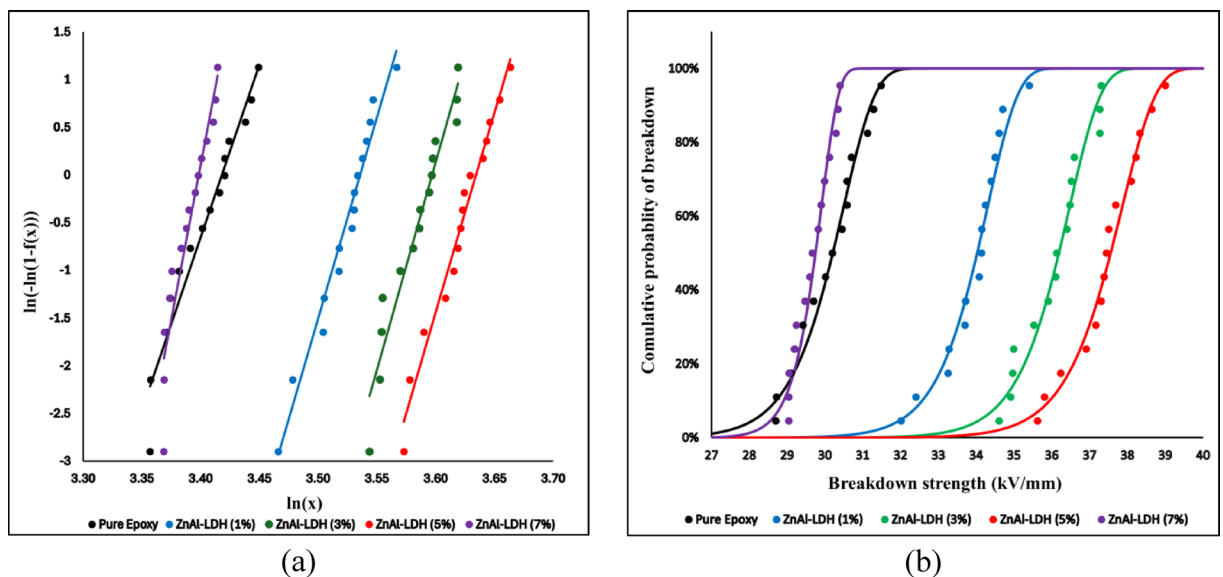


Fig. 19. The logarithmic and linear scale Weibull plot of all material samples.

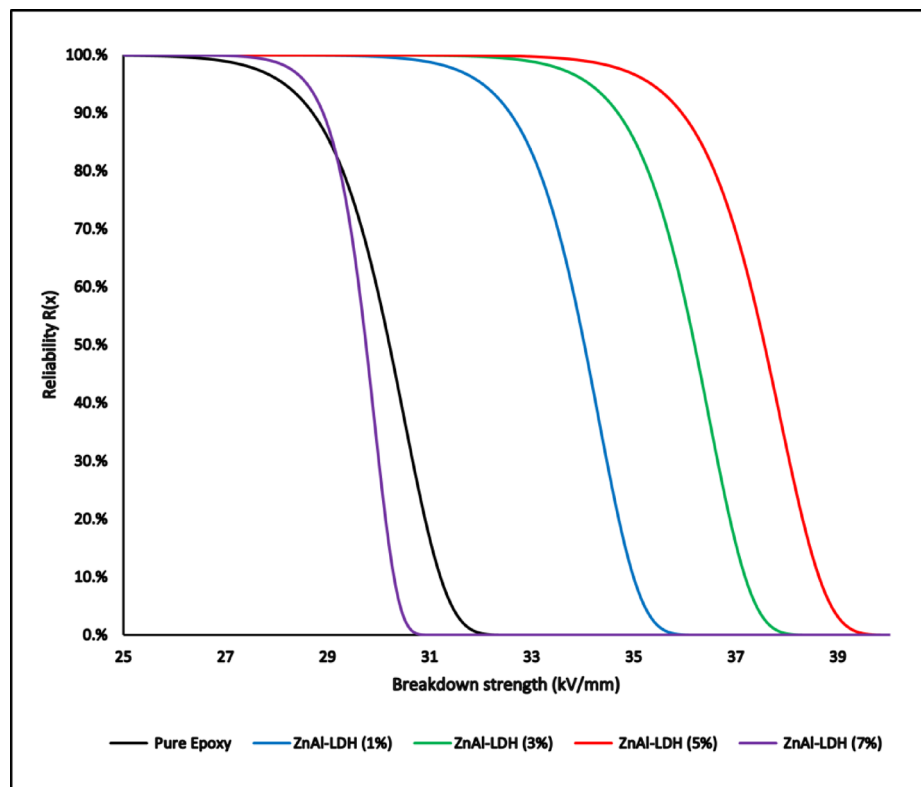


Fig. 20. The Weibull reliability curves of all materials.

- high adsorption capacity and effective charge-trapping capability, both advantageous for electrical insulation.
- The SEM/EDX validated the presence of Zn and Al uniformly distributed in the polymeric background with confirmation of the successful incorporation of LDH into the epoxy matrix, increasing structural ordering from 21.1% for neat epoxy to 28.9% for 5 wt.% composite.
 - TGA showed improved thermal stability: char residue increased from 14% for neat epoxy to 17.1% for 5 wt.% composite. DSC revealed an increase in glass transition temperature from 93.5 °C to 109.8 °C at 5 wt.%, surpassing the IEC 62271-1 operational requirement of 105 °C.
 - Relative permittivity (ϵ') improved slightly at 1–3 wt.% but declined at higher loadings (5–7 wt.%) due to interfacial constraints and agglomeration. Dielectric loss ($\tan \delta$) stayed within safe limits at 50 Hz, and AC conductivity was suppressed to 10^{-8} S/cm, confirming strong insulating performance
 - The breakdown strength improved steadily with fillers loading up to 5 wt.%, reaching 37.4 kV/mm, which is $\approx 24\%$ higher than that of neat epoxy. At this level, the composite also showed the most consistent performance. Beyond 5 wt%, however, agglomeration effects dominated, and the strength dropped below that of pure epoxy. Thus, the optimum loading is clearly at 5 wt.%.

Although the results confirm the significant potential of Zn/Al-LDH/epoxy nanocomposites for high-voltage insulation applications, this study was limited to short-term laboratory conditions. Further research is needed to evaluate the long-term aging stability, humidity influence, and electrical endurance under service-like stress environments. Such investigations would provide deeper insight into the reliability and field applicability of LDH-based epoxy materials in GIS/GITL systems.

Data availability

Data is available with all authors and will be made accessible to others upon reasonable request.

Received: 16 September 2025; Accepted: 26 December 2025

Published online: 27 January 2026

References

- Xing, Y. et al. Defects and failure types of solid insulation in gas-insulated switchgear: In situ study and case analysis. *High Volt.* 7(1), 158–164. <https://doi.org/10.1049/hve2.12127> (2022).
- Hari, R. & Mohana Rao, M. Characterization of nano-additive filled epoxy resin composites (ERC) for high voltage gas insulated switchgear (GIS) applications. *Int. J. Emerg. Electr. Power Syst.* 23(1), 47–57. <https://doi.org/10.1515/ijeeps-2020-0257> (2022).
- Alsoud, A. et al. Electrical characterization of epoxy nanocomposite under high DC voltage. *Polymers* <https://doi.org/10.3390/polym16070963> (2024).

4. Al Soud, A., Daradkeh, S. I., Knápek, A., Holcman, V. & Sobola, D. Electrical characteristics of different concentration of silica nanoparticles embedded in epoxy resin. *Phys. Scr.* <https://doi.org/10.1088/1402-4896/ad070c> (2023).
5. Sundar, U., Lao, Z. & Cook-Chennault, K. Enhanced dielectric permittivity of optimized surface modified of barium titanate nanocomposites. *Polymers* <https://doi.org/10.3390/POLYM12040827> (2020).
6. Adnan, M. M. et al. Epoxy-based nanocomposites for high-voltage insulation: A review. *Adv. Electr. Mater.* <https://doi.org/10.1002/aelm.201800505> (2019).
7. Al Soud, A., Daradkeh, S., Knápek, A., Liedermann, K., Holcman, V. & Sobola, D. Influence of High Concentration of Silica Nanoparticles on the Dielectric Spectra. In *Proceedings II of the Conference Student EEICT*, Brno University of Technology. (2023). <https://doi.org/10.13164/eeict.2023.253>.
8. Abdullah, A. Q. Dielectric Properties of Epoxy/Al₂O₃Nanocomposites. *Int. J. Appl. Innov. Eng. Manag.* (2014). [Online]. Available: <https://www.researchgate.net/publication/326112263>
9. Ye, T. et al. MgAl LDH nanosheets loaded with Ni nanoparticles: a multifunctional filler for improving the energy storage performance of PVDF-based nanocomposites. *RSC Adv.* **11**(31), 19128–19135. <https://doi.org/10.1039/d1ra01570b> (2021).
10. Huan, X. et al. Enhancing electrical insulation of epoxy composites by suppressing charge injection and subsequently electric field distortion. *Compos. Commun.* <https://doi.org/10.1016/j.coco.2025.102391> (2025).
11. Liu, T. et al. Multifunctional epoxy coatings reinforced with LDHs-modified silica microspheres: Synergistic effects on corrosion resistance, thermal insulation, and flame retardancy. *Colloids Surf A: Physicochem. Eng. Aspects* <https://doi.org/10.1016/j.colsurfa.2024.134578> (2024).
12. Said, A., Ezzat, M., Abd-Allah, M. A., El-Gamal, S. M. A. & Ramadan, M. Charge dynamics and flashover performance enhancement of GIS spacers via ZnAl-LDH/Epoxy nanocomposites: Experimental and simulation perspectives. *Electr. Power Syst. Res.* **252**, 112438. <https://doi.org/10.1016/j.epsr.2025.112438> (2026).
13. Said, A., Abd-Allah, M. A., Nawar, A. G., Elsayed, A. E. & Kamel, S. Enhancing the electrical and physical nature of high-voltage XLPE cable dielectric using different nanoparticles. *J. Mater. Sci.: Mater. Electron.* **33**(10), 7435–7443. <https://doi.org/10.1007/s10854-022-07868-9> (2022).
14. Chowdhury, A. et al. Controlling reaction kinetics of layered zinc vanadate having brucite-like Zn–O layers supported by pyrovanadate pillars for use in supercapacitors. *J. Alloy. Compd.* **829**, 154479. <https://doi.org/10.1016/J.JALLCOM.2020.154479> (2020).
15. Mohsen, A., Amin, M. S., Selim, F. A. & Ramadan, M. The impact of wurtzite and mesoporous Zn–Al–CO₃ LDH on the performance of alkali-activated-slag: Setting times, compressive strength, and radiation attenuation. *Constr. Build. Mater.* **438**, 137218. <https://doi.org/10.1016/J.CONBUILDMAT.2024.137218> (2024).
16. Ramadan, M., Sayed, D. G. & Selim, F. A. Exploration of fungal resistivity and mechanical performance of Zn-phases-doped geopolymers: ZnO and Zn/Al-LDH nanoparticles. *Constr. Build. Mater.* **457**, 139369. <https://doi.org/10.1016/J.CONBUILDMAT.2024.139369> (2024).
17. Karlsson, M. E. et al. Lamellae-controlled electrical properties of polyethylene-morphology, oxidation and effects of antioxidant on the DC conductivity. *RSC Adv.* **10**(8), 4698–4709. <https://doi.org/10.1039/c9ra09479b> (2020).
18. Tsen, A. W. et al. Tailoring electrical transport across grain boundaries in polycrystalline graphene. *Science* **336**(6085), 1143–1146. <https://doi.org/10.1126/science.1218948> (2012).
19. Cheng, L. et al. High-performance Al₂O₃/polyarylate nanocomposite paper with enhanced Insulation, thermal conductivity, and environmental stability for advanced electrical applications. *Chem. Eng. J.* **511**, 162000. <https://doi.org/10.1016/J.CEJ.2025.162000> (2025).
20. Wang, X. et al. Large-surface-area BN nanosheets and their utilization in polymeric composites with improved thermal and dielectric properties. *Nanoscale Res. Lett.* <https://doi.org/10.1186/1556-276X-7-662> (2012).
21. Mashkoo, F., Shoeb, M., Khan, M. N. & Jeong, C. Facile synthesis of polypyrrole-decorated RGO-CuS nanocomposite for efficient nickel removal from wastewater. *Polymers* <https://doi.org/10.3390/polym16223138> (2024).
22. Sabukuttan, D. et al. Hydrothermal synthesis and physicochemical characterization of carbon quantum dots from marine cyanobacteria leptolyngbya sp. nov. KMBMA-1. *Bionanoscience*. <https://doi.org/10.1007/s12668-025-02015-0> (2025).
23. Mohsen, A., Amin, M. S. & Ramadan, M. Synthesis of highly efficient microwaved geopolymer based on alkaline activation of slag/bentonite precursors: The correlation among hydraulic phases, porosity profile, and compressive strength. *Constr. Build. Mater.* **476**, 141299. <https://doi.org/10.1016/J.CONBUILDMAT.2025.141299> (2025).
24. Mohsen, A. et al. Correlation between porous structure analysis, mechanical efficiency and gamma-ray attenuation power for hydrothermally treated slag-glass waste-based geopolymer. *Case Stud. Constr. Mater.* **17**, e01505. <https://doi.org/10.1016/J.CSCM.2022.E01505> (2022).
25. Mohsen, A. et al. Bio-mechanical efficacy for slag/fly ash-based geopolymer mingled with mesoporous NiO. *Case Stud. Constr. Mater.* **19**, e02283. <https://doi.org/10.1016/J.CSCM.2023.E02283> (2023).
26. Mohsen, A., Ramadan, M., Habib, A. O. & Abdel-Gawwad, H. A. Evaluating the role of magnesium aluminate nano spinel in phase composition, meso-porosity, compressive strength, and drying shrinkage of alkali-activated slag. *Constr. Build. Mater.* **409**, 133857. <https://doi.org/10.1016/J.CONBUILDMAT.2023.133857> (2023).
27. Ramadan, M., Amin, M. S., Selim, F. A. & Mohsen, A. Upgrading physico-mechanical characteristics and bacterial resistivity for cementless pastes modified with ZnAl₂O₄ nano-spinel: A comparative study with ZnO. *J. Build. Eng.* **97**, 110700. <https://doi.org/10.1016/J.JOBE.2024.110700> (2024).
28. Ramadan, M. et al. De-aluminated metakaolin-cement composite modified with commercial titania as a new green building material for gamma-ray shielding applications. *Case Stud. Constr. Mater.* **17**, e01344. <https://doi.org/10.1016/J.CSCM.2022.E01344> (2022).
29. Pradhan, S. et al. Elastomer/LDH nanocomposites: Synthesis and studies on nanoparticle dispersion, mechanical properties and interfacial adhesion. *Eur. Polymer J.* **44**(10), 3122–3132. <https://doi.org/10.1016/J.EURPOLYMJ.2008.07.025> (2008).
30. Timoshenko, V. Y., Dittrich, T., Koch, F., Lisachenko, M. G. & Lysenko, V. Free charge carriers in mesoporous silicon. *Phys. Rev. B* <https://doi.org/10.1103/PhysRevB.64.085314> (2001).
31. Leijtens, T. et al. Electronic properties of meso-superstructured and planar organometal halide perovskite films: Charge trapping, photodoping, and carrier mobility. *ACS Nano* <https://doi.org/10.1021/nn502115k> (2014).
32. Sen, T. & Barisik, M. Pore connectivity effects on the internal surface electric charge of mesoporous silica. *Colloid Polym. Sci.* <https://doi.org/10.1007/s00396-019-04555-w> (2019).
33. Liu, S. et al. Expanded properties and applications of porous flame-retardant polymers containing graphene and its derivatives. *Multidiscip. Digit. Publ. Inst. (MDPI)* <https://doi.org/10.3390/polym16142053> (2024).
34. Sabu, M., Bementa, E., Ruban, Y. & G. Mon S.,. A novel analysis of the dielectric properties of hybrid epoxy composites. *Adv. Compos. Hybrid Mater.* <https://doi.org/10.1007/s42114-020-00166-0> (2020).
35. Aminifazl, A., Karunarathne, D. J. & Golden, T. D. Synthesis of silane functionalized LDH-modified nanopowders to improve compatibility and enhance corrosion protection for epoxy coatings. *Molecules* <https://doi.org/10.3390/molecules29040819> (2024).
36. Zhang, Y. et al. Bioinspired LDH-based hierarchical structural hybrid materials with adjustable mechanical performance. *Adv. Funct. Mater.* <https://doi.org/10.1002/adfm.201801614> (2018).
37. Omar, H. et al. Calorimetric and dielectric investigations of epoxy-based nanocomposites with halloysite nanotubes as nanofillers. *Polymers* <https://doi.org/10.3390/polym13101634> (2021).

38. Lakshmaiya, N. et al. Influence of oil palm nano filler on interlaminar shear and dynamic mechanical properties of flax/epoxy-based hybrid nanocomposites under cryogenic condition. *Coatings* <https://doi.org/10.3390/coatings12111675> (2022).
39. Oner, G., Nadaroglu, H., Acar, V. & Gok, S. Flexural and thermal characterization of epoxy composites reinforced with nanoparticles synthesized from waste walnut husk with green synthesis method. *Biomass Convers. Biorefinery* **14**, 1–12. <https://doi.org/10.1007/s13399-023-04364-w> (2023).
40. Iderus, S., Peter, G. & Vivekananda, G. An innovative method to conduct temperature rise test on medium voltage switchgear assembly based on IEC standards in a power grid. *J Eng.* <https://doi.org/10.1049/tje2.12166> (2022).
41. Li, Q. et al. DeoxyriboNucleic acid-enhanced carbon nanotube dispersed epoxy resin composites: Mechanical and thermal properties study. *Polym. Compos.* **45**, 15857–15877. <https://doi.org/10.1002/pc.28875> (2024).
42. Guo, Q., Wang, T., Ouyang, L. & Yuan, S. Superhydrophobic double layered MgAl-LDH/epoxy composite coatings for enhanced anticorrosion performance of magnesium alloys. *Prog. Org. Coat.* **174**, 107300. <https://doi.org/10.1016/j.porgcoat.2022.107300> (2023).
43. Xia, X., Zhong, Z. & Weng, G. J. Maxwell–wagner–sillars mechanism in the frequency dependence of electrical conductivity and dielectric permittivity of graphene-polymer nanocomposites. *Mech. Mater.* **109**, 42–50. <https://doi.org/10.1016/j.mechmat.2017.03.014> (2017).
44. Schönhals, A., Goering, H., Costa, F. R., Wagenknecht, U. & Heinrich, G. Dielectric properties of nanocomposites based on polyethylene and layered double hydroxide. *Macromolecules* **42**(12), 4165–4174. <https://doi.org/10.1021/ma900077w> (2009).
45. Wang, L., Yang, J., Cheng, W., Zou, J. & Zhao, D. Progress on polymer composites with low dielectric constant and low dielectric loss for high-frequency signal transmission. *Front. Mater.* <https://doi.org/10.3389/fmats.2021.774843> (2021).

Author contributions

All the authors contributed equally to this work. M. Ramadan Conceptualization, Writing—original draft, Methodology, Investigation, Software, Writing—review & editing, Data curation, Visualization. Mahmoud Ez-zat Writing—original draft, Methodology, Investigation, Software, Writing—review & editing, Data curation, Visualization. Mousa. A. Abd-Allah Conceptualization, review & editing, Data curation, Visualization. S. M. A. El-Gamal Conceptualization, review & editing, Data curation, Visualization. Abdelrahman Said Conceptualization, Writing—original draft, Methodology, Investigation, Software, Writing—review & editing, Data curation, Visualization.

Funding

Open access funding provided by The Science, Technology & Innovation Funding Authority (STDF) in cooperation with The Egyptian Knowledge Bank (EKB).

Declarations

Competing interests

The authors declare no competing interests.

Additional information

Correspondence and requests for materials should be addressed to M.R. or A.S.

Reprints and permissions information is available at www.nature.com/reprints.

Publisher's note Springer Nature remains neutral with regard to jurisdictional claims in published maps and institutional affiliations.

Open Access This article is licensed under a Creative Commons Attribution 4.0 International License, which permits use, sharing, adaptation, distribution and reproduction in any medium or format, as long as you give appropriate credit to the original author(s) and the source, provide a link to the Creative Commons licence, and indicate if changes were made. The images or other third party material in this article are included in the article's Creative Commons licence, unless indicated otherwise in a credit line to the material. If material is not included in the article's Creative Commons licence and your intended use is not permitted by statutory regulation or exceeds the permitted use, you will need to obtain permission directly from the copyright holder. To view a copy of this licence, visit <http://creativecommons.org/licenses/by/4.0/>.

© The Author(s) 2026